Am J Cancer Res 2021;11(6):2590-2617
www.ajcr.us /ISSN:2156-6976/ajcr0131974

Original Article

A preclinical report of a cobimetinib-inspired novel anticancer small-molecule scaffold of isoflavones, NSC777213, for targeting PI3K/AKT/mTOR/MEK in multiple cancers

Bashir Lawal[1,2*], Wen-Cheng Lo[3,4,5*], Ntlotlang Mokgautsi[1,2], Maryam Rachmawati Sumitra[1,2], Harshita Khedkar[1,2], Alexander TH Wu[6,7,8,9], Hsu-Shan Huang[1,2,10,11]

[1]PhD Program for Cancer Molecular Biology and Drug Discovery, College of Medical Science and Technology, Taipei Medical University and Academia Sinica, Taipei 11031, Taiwan; [2]Graduate Institute for Cancer Biology & Drug Discovery, College of Medical Science and Technology, Taipei Medical University, Taipei 11031, Taiwan; [3]Department of Surgery, Division of Neurosurgery, School of Medicine, College of Medicine, Taipei Medical University, Taipei 11031, Taiwan; [4]Department of Neurosurgery, Taipei Medical University Hospital, Taipei 11031, Taiwan; [5]Taipei Neuroscience Institute, Taipei Medical University, Taipei 11031, Taiwan; [6]TMU Research Center of Cancer Translational Medicine, Taipei Medical University, Taipei 11031, Taiwan; [7]The PhD Program of Translational Medicine, College of Science and Technology, Taipei Medical University, Taipei 11031, Taiwan; [8]Clinical Research Center, Taipei Medical University Hospital, Taipei Medical University, Taipei 11031, Taiwan; [9]Graduate Institute of Medical Sciences, National Defense Medical Center, Taipei 11490, Taiwan; [10]School of Pharmacy, National Defense Medical Center, Taipei 11490, Taiwan; [11]PhD Program in Biotechnology Research and Development, College of Pharmacy, Taipei Medical University, Taipei 11031, Taiwan. [*]Equal contributors.

Received February 17, 2021; Accepted May 14, 2021; Epub June 15, 2021; Published June 30, 2021

Abstract: The phosphatidylinositol 3-kinase (PI3K)/protein kinase B/mammalian target of rapamycin (mTOR) and mitogen-activated protein kinase kinase/extracellular signal-regulated kinase (MEK/ERK) signaling pathways are critical for normal human physiology, and any alteration in their regulation leads to several human cancers. These pathways are well interconnected and share a survival mechanism for escaping the depressant effect of antagonists. Therefore, novel small molecules capable of targeting both pathways with minimal or no toxicity are better alternatives to current drugs, which are disadvantaged by their accompanying resistance and toxicity. In this study, we demonstrate that the PI3K/AKT/mTOR/MEK is a crucial oncoimmune signature in multiple cancers. Moreover, we describe NSC777213, a novel isoflavone core and cobimetinib-inspired small molecule, which exhibit both antiproliferative activities against all panels of NCI60 human tumor cell lines (except COLO205 and HT29) and a selective cytotoxic preference for melanoma, non-small-cell lung cancer (NSCLC), brain, renal, and ovarian cancer cell lines. Notably, for NSC777213 treatment, chemoresistant ovarian cancer cell lines, including SK-OV-3, OVCAR-3, OVCAR-4, and NCI/ADR-RES, exhibited a higher antiproliferative sensitivity (total growth inhibition (TGI) = 7.62-31.50 μM) than did the parental cell lines OVCAR-8 and IGROV1 (TGI > 100 μM). NSC777213 had a mechanistic correlation with clinical inhibitors of PI3K/AKT/mTOR/MEK. NSC777213 demonstrates robust binding interactions and higher affinities for AKT and mTOR than did isoflavone, and also demonstrate a higher affinity for human MEK-1 kinase than some MEK inhibitors under clinical developments. In addition, treatment of U251 and U87MG cells with NSC777213 significantly downregulated the expression levels of the total and phosphorylated forms of PI3K/AKT/mTOR/MEK. Our study suggests that NSC777213 is a promising PI3K/AKT/mTOR/MEK inhibitor for further preclinical and clinical evaluation as a chemotherapeutic agent, particularly for the treatment of NSCLC, melanoma, and brain, renal, and ovarian cancers.

Keywords: PI3K/AKT/mTOR-MEK pathways, NSC777213, NCI60 human tumor cell lines, immune infiltrations, anticancer activities, molecular docking simulations

Introduction

The phosphatidylinositol 3-kinase (PI3K)/protein kinase B/mammalian target of rapamycin (mTOR) pathway is a crucial intracellular signaling pathway that plays a vital regulatory role in metabolism and cell cycle [1, 2]. Alterations of this signaling pathway is a common event that

contributes to the cell survival and proliferation, angiogenesis, tumorigenesis, and metastasis of almost all human malignancies [3, 4]. PI3K is a heterodimer protein consisting of p85 regulatory and p110 catalytic subunits [5]. PI3K pathway dysregulation occurs either through gene amplification or mutations and induces a myriad of downstream effectors, leading to the development and progression of cancers [2, 6]. Activated PI3K phosphorylates phosphatidylinositol-4,5-bisphosphate to phosphatidylinositol-3,4,5-triphosphate [1, 7]. Once phosphorylated, PI3K activates AKT, which regulates several downstream molecules, including mTOR [2, 7]. Moreover, AKT may be activated due to mutation in the AKT PH domain and a loss of PTEN, a tumor suppressor gene; such activation may also be due to inositol polyphosphate-4-phosphatase type II, an enzyme that negatively regulates PI3K through phosphatidylinositol-3,4,5-triphosphate dephosphorylation [8, 9]. The activated AKT in turn phosphorylates mTOR, which activates mTOR complex 1 (mTORC1) and mTOR complex 2 (mTORC2), two protein complexes with distinct structures, functions, and substrate specificities [10, 11].

The mTORC1 comprises mTOR, DEPTOR, Raptor, PRAS40, and mLST8, whereas the mTORC2 comprises mTOR, DEPTOR, Proctor, Rictor, mSin1, and mLST8 [12, 13], with mTOR being the catalytic subunit of both complexes. The mTORC1 is the downstream component of the PI3K-AKT pathway that regulates cellular processes through signal integration from growth factor receptors, tumor suppressors, oncoproteins, and the intracellular nutrient status [1, 14]. The mTORC1 regulates protein synthesis and turnover through the phosphorylation of eIF4E binding protein 1 and ribosomal protein S6 kinase (S6K), which in turn enhances glycolytic pathway and protein biosynthesis to initiate metabolic remodeling and regulate translation initiation [15, 16]. Conversely, the mTORC2 plays a role in AKT-mediated cell survival and migration independent of mTORC1 activity [17]. mTOR regulates hypoxia-inducible factor 1, vascular endothelial growth factor, cyclin D1, and cell transitions from the G1 to S phases, enhancing rapid cell proliferation and the growth and survival of many tumors [18]. In addition, mTOR/S6K can upregulate many pro-angiogenic factors, such as AP-1, to promote carcinogenesis [19, 20]. Because mTOR plays various roles in tumorigenic promotion, mTOR hyperactivation occurs in approximately 70% of human tumors, and this activation is often associated with therapy resistance and overall poor prognosis [19, 21]. Ras/Raf/MEK/extracellular regulated kinase (ERK) is a crucial signaling pathway for normal human physiological processes, and alteration in the regulation of this pathway leads to cancers [2]. MEK promotes cell proliferation, cell survival, and metastasis through ERK phosphorylation, which in turn translocates to the nucleus to regulate gene expression and various transcription factors [22].

Rapamycin and its analogs have been reported to inhibit mTORC1 activity and have demonstrated some levels of effectiveness as a monotherapy agent [11, 23]. However, many studies have reported resistance to these drugs owing to the activation of mTORC2 and PI3K signaling pathways [24]. In addition, although mTORC1 and mTORC2 inhibition can lead to the decreased phosphorylation of AKT, mTOR inhibitors may unexpectedly upregulate the PI3K/PDK1 pathway [9, 24]. Therefore, the concomitant inhibition of both PI3K and mTOR may offer a better anticancer response compared with the targeting of mTOR alone. However, pan-specific PI3K/AKT/mTOR inhibitors are effective at high doses, and their overall success in clinical trials has been limited by toxicity problems, including immunosuppression, hepatic impairment, pneumonitis, hypo- and hyperglycemia, mouth ulcers, constipation, cardiac toxicity, cutaneous reactions, neuropsychiatric defeats, nausea, diarrhea, and colitis [20, 25-27]. These adverse effects are limiting factors in administrating the most effective dosages. Therefore, using natural products for therapeutic intervention has attracted renewed interest owing of their ability to modulate multiple pathways and their nontoxic properties in contrast to conventional therapy [28-32]. Isoflavone derivatives are potent inhibitors of the PI3K/AKT/mTOR signaling pathway [33, 34]. In addition, isoflavones have been reported to sensitize cancer cells to radiation therapy and work in synergy with conventional chemotherapy in multiple cancers [33, 34].

However, increasing evidence has suggested that the PI3K/AKT/mTOR and Raf/MEK/ERK pathways intersect at multiple junctions, exhibit crosstalk, and contain feedback loops [8]. Inhibiting one pathway can result in signaling

maintenance through the other pathway. The existence of such mutual survival mechanisms implies that the dual targeting of these pathways may offer higher efficacy and better clinical outcomes compared with targeting one of the pathways. In the present study, we used a fragment-based drug design strategy to develop NSC777213, a novel, isoflavone-core small molecule derivative of cobimetinib. Furthermore, we demonstrated its anticancer activities in multiple cancers using the well characterized NCI60 panels of human tumor cell lines and provided *in silico* and structure-based mechanistic evidence for targeting PI3K/AKT/mTOR/MEK signatures.

Materials and methods

Clinical data retrieval and analysis

We used the UALCAN portal [35] to analyzed the differential gene expression profile of PI3K/AKT/mTOR/MEK between tumor samples and adjacent normal tissue across TCGA cancers. We used GEPIA2, an interactive web server for analyzing the RNA sequencing expression [36] to query the correlation between the expression of PI3K/AKT/mTOR and MEK expression in TCGA cancer. The correlation of PI3K/AKT/mTOR/MEK with tumor immune infiltrations and cancer associated fibroblast infiltrations were analyzed using the Tumor IMmune Estimation Resource (TIMER2.0) resource (http://timer.cistrome.org/) [37].

Functional enrichment and PPI network analysis

We performed the enrichment analysis of PI3K/AKT/mTOR/MEK signature to identified the Kyoto Encyclopedia of Genes (KEGG) pathways and gene ontologies enriched by the signature, while the protein-protein interaction (PPI) analysis was performed using the STRING server (string-db.org/). Significant enrichment was considered when $p\text{-value} < 0.05$.

Analysis of prognostic relevance

To analyzed the prognostic relevance of PI3K/AKT/mTOR/MEK, we performed survival analysis on TRGAted using the survival (v2.41-3) and survminer (v0.4.2) R packages. Optimal cutpoints are based on the surv_cutpoint function in the survminer package, finding the lowest log-rank *p*-value with the minimum proportional comparison set to 15% versus 85% of samples. Hazard ratios are derived from the Cox Proportional Hazard regression model and are based on the High-versus-Low comparison. Outputs are the hazard ratios for each protein and -log10 *P*-value based on the Cox Regression calculations for the overall survival, disease-free survival, and disease progressive free survival of the cohorts.

Analysis of NSC777213's biological activity, pharmacokinetics, drug likeness, toxicity, and medicinal chemistry

A computer-aided Prediction of Biological Activity Spectra (PASS) web resource (http://way2drug.com/dr) was used to predict the biological activities of NSC777213 [38]. The physicochemical properties, medicinal chemistry, pharmacokinetics, and drug likeness of NSC777213 were analyzed using the SwissADME algorithm of the Swiss Institute of Bioinformatics (http://www.swissadme.ch) [39]. Drug likeness was analyzed considering the Lipinski (Pfizer) rule of five [40]. The probability of the oral bioavailability of the compound in rats or the compound's measurable Caco-2 permeability was estimated using the Abbot Bioavailability Score [41], whereas the Brain Or IntestinaL EstimateD permeation (BOILED-Egg) model [42] was used to evaluate gastrointestinal absorption and blood-brain permeation ability. Acute toxicity (LD_{50}) in rats and environmental toxicity were predicted using GUSAR software [43].

In vitro anticancer screening of NSC777213

The in vitro anticancer activities of NSC777213 was screened for at the US National Cancer Institute (NCI) against 60 panels of cancer cell lines representing nine major human cancers, namely leukemia, melanomas, non-small-cell lung carcinoma (NSCLC), brain, ovarian, kidney, breast, colon and prostate cancer, according to established protocols (http://dtp.nci.nih.gov). Initially, NSC777213 was evaluated at a single dose of 10 Mm. Following satisfactory results in the single-dose assay, NSC777213 was further evaluated for five-dose screening against the same cell line panels. According to the protocols [44, 45], varying amounts of cells ranging from 5,000-40,000 (selected on the basis of doubling time) were seeded for 24 h into each well of 96-well plates. Cells were treated with NSC765598 at a concentration of 10 μM in the case of either a single-dose assay or five

doses (0, 0.1, 1.0, 10, and 100 μM) for a dose-dependent assay and incubated for 48 h at 37°C and 5% humidified CO_2. Cell viability was determined using the sulforhodamine B solution protocol [46]. Growth inhibition was calculated in relation to cells without drug treatment and the time-zero control. Results of the multiple-dose assay are represented in terms of the NSC777213 concentrations that cause 50% growth inhibition (GI_{50}), total growth inhibition [47], and 50% cell lethality (LC_{50}) [48].

NSC777213 drug target and mechanistic identification

We used the NCI-COMPARE analysis (https://dtp.cancer.gov/databases_tools/compare.htm) to correlate the anticancer fingerprints of NSC777213 with NCI synthetic compounds, investigational drugs, marketed drugs, and standard agents. Because the NCI cell lines used in this study are well characterized, we correlated the anticancer fingerprints of NSC777213 with the expression of molecular targets in the cell lines [49]. The NSC numerical IDs were used as the "seed", whereas GI_{50}, TGI, and LC_{50} were set as the endpoints [50]. In addition, we screened NSC777213 for potential drug targets by using in silico algorithms, including the SwissTargetPrediction algorithm (http://www.swisstargetprediction.ch/), which predicts potential drug targets based on the similarity principle [51], and the PharmMapper Server, a pharmacophore mapping algorithm with statistical modules (http://lilab-ecust.cn/pharmmapper/index.html) [52].

Western blot analysis

An established protocol for the Western blot analysis [53] was used to analyze the suppressive effect of NSC777213 on the expression levels of PI3K/AKT/mTOR/MEK. Following treatment with NSC777213 (2 μM) for 48 hr, total protein lysates from cells were separated by 10% sodium dodecylsulfate polyacrylamide gel electrophoresis (SDS-PAGE), transferred onto polyvinylidene difluoride membranes (Bio-Rad Laboratories, Hercules, CA, USA), and blocked (with 5% skimmed milk) for non-specific binding. Finally, the membrane was immunoblotted with primary antibodies; AKT (#9272, 1:1000), p-AKT (#4060 1:1000), MEK1 (#E11-7147B, 1:1000), p-MEK1 (#E11-7147A, 1:1000), mTOR (#2983, 1:1000), p-mTOR (#2974, 1:1000), p-PI3K (#E11-1224A, 1:1000), and GAPDH (#ARG10112, 1:5000) for 15 h, and secondary antibodies (horseradish peroxidase-linked anti-rabbit and mouse, 1:5000) for 2 h. Protein signals from the membrane were detected with an enhanced chemiluminescence kit (Thermo Fisher Scientific, Waltham, MA, USA).

Molecular docking simulation of NSC777213 with the targets

The three-dimensional (3D) structure of pimasertib (CID: 44187362), refametinib (CID: 44182295), cobimetinib (CID: 16222096), mirdametinib (CID: 9826528) (phase I), and TAK733 (CID: 24963252) was retrieved in the SDF file format from the PubChem database, whereas the 3D structures of NSC777213 were obtained in the Sybyl mol2 format using the Avogadro molecular builder and visualization tool version 1.XX [54] before being subsequently transformed into the protein data bank (PDB) format using the PyMOL Molecular Graphics System, version 1.2r3pre. The PDB files of the crystal structures of the receptors including the human mTOR complex 1 (PDB: 5FLC), AKT kinase domain (PDB: 1GZN), human PI3K-gamma (PDB: 3APC) and human MEK-1 kinase (PDB; 5YYX) were retrieved from the PDB. All PDB files were subsequently converted into pdbqt format by using AutoDock VINA (version 0.8) [55]. Before docking, we removed water molecules, added hydrogen, and charged the receptor. Docking was conducted using AutoDock VINA software per a method described in previous study [56, 57]. The PyMOL software and Discovery studio visualizer (version 19.1.0.18287, BIOVIA, San Diego, CA, USA) [58] were used to visualize the docked complex and analyze the interactions. Furthermore, we used Swiss dock, an online docking algorithm [59], to dock and evaluate the binding affinity of NSC777213 to the target.

Data analysis and visualization

GraphPad software (version 8) was used for data analysis. The statistical significance of differentially expressed genes was evaluated using the Wilcoxon test. Kaplan-Meier survival plots was used for visualizing the overall survival of the cohorts. Growth inhibition by NSC765598 in the single-dose assay was obtained through the subtraction of the positive value on the plot from 100, that is, a value of 40 indicates 60% growth inhibition. Spearman's rank correlation was used to

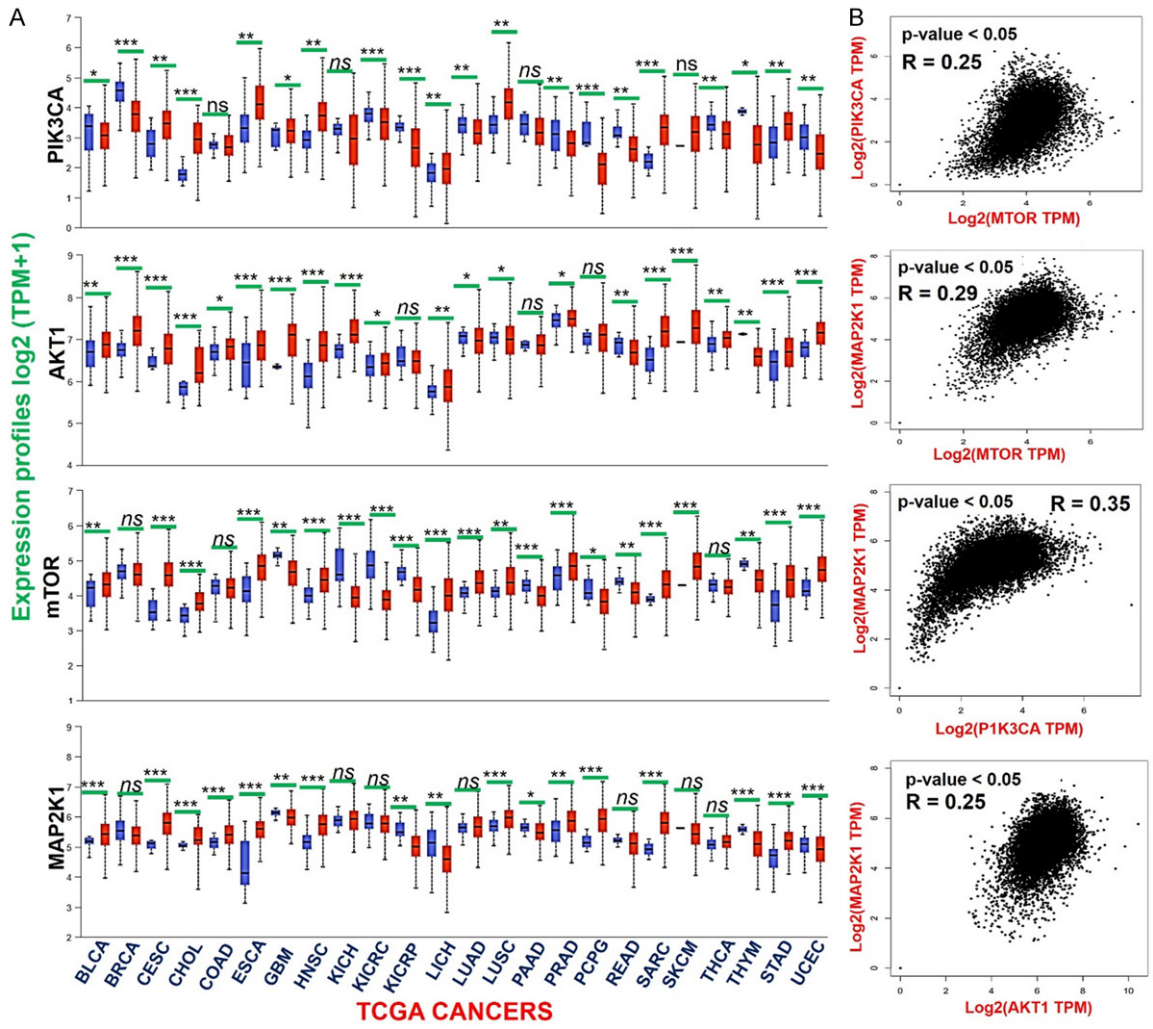

Figure 1. PI3K/AKT/mTOR-MEK is overexpressed in multiple cancer. A. Differential expression of PI3K/AKT/mTOR-MEK between tumor sample and adjacent normal tissue across TCGA cancers. The red bars represent the tumor sample while the blue bars represent the normal tissue. B. Scatterplots showing the mRNA expression correlation between PI3K/AKT/mTOR and MEK in 9,736 TCGA cancer cohorts. A non-log scale was used for calculation and a log-scale axis for visualization.

assess the correlations of NSC777213 anticancer fingerprints with NCI database compounds and molecular targets. The COMPARE correlation threshold was set to ≥45 common cell lines, a ≥0.1 correlation coefficient, and a ≥0.05 standard deviation, with the significance levels of $P < 0.05$, < 0.01, and < 0.001, respectively.

Results and discussions

PI3K/AKT/mTOR/MEK is overexpressed in multiple cancers and is associated with a worse prognosis of cancer cohorts

Various studies have shown the importance of molecular biomarkers in the diagnosis, prognosis, prediction, and targeted therapy of diseases [60]. In the present study, we queried the differential expression profile of PI3K/AKT/mTOR-MEK between 9,736 tumors and 8,587 normal samples across TCGA cancers and found that the mRNA of PI3K/AKT/mTOR/MEK is expressed at high levels in tumor samples of different cancer type than the corresponding adjacent normal tissue (**Figure 1A**). In addition, we found that expression of PI3K/AKT/mTOR correlates positively ($r > 0.25$) with MEK expression in TCGA cancer cohorts available within GEPIA2 (**Figure 1B**). These results are consistent with previous reports showing that PI3K-Akt signaling pathways are over-expressed in about 70% of all cancer types. Importantly, our

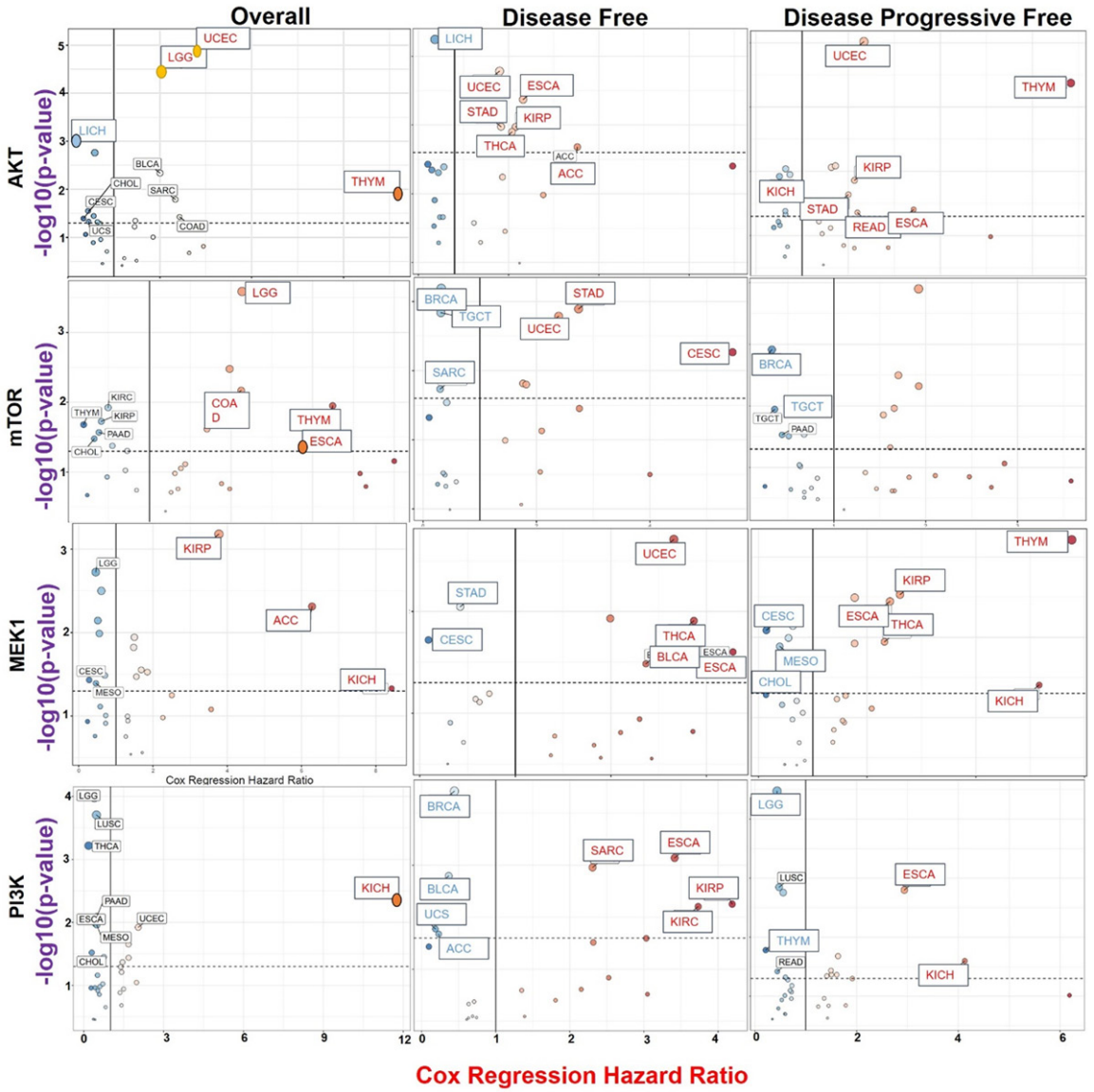

Figure 2. PI3K/AKT/mTOR/MEK expression is associated with poor prognosis of multiple cancer cohorts. Volcano plot showing the cox regression hazard ratio of overall survival, disease-free survival, and disease progressive free survival of cancer cohorts with differentially expressed PI3K/AKT/mTOR/MEK.

results revealed the associations between the overexpression of this signature and worse prognosis in multiple cancer cohorts (**Figure 2**). COX regression analysis indicated that PI3K expression is associated with worse overall survival of KICH; disease-free survival of SARC, ESCA, KIRC, and KIRP; and disease progressive free survival of ESCA and KICH cohorts. AKT expression is associated with worse overall survival of COAD, BLCA, LGG, UCEC, and THYM; disease-free survival of UCEC, STAD, KIRP, THCA, ACC, and ESCA; and disease progressive free survival of UCEC, STAD, KIRP, READ, ESCA and THYM cohorts. mTOR expression is associated with worse overall survival of COAD, LGG, UCS, and ESCA, and disease-free survival of UCEC, STAD and CESC cohorts while MEK1 expression is associated with worse overall survival of KIRP, ACC, and KICH; disease-free survival of UCEC, BLCA, THCA and ESCA; and disease progressive free survival of ESCA, KIRP, THCA, KICH and THYM cohorts (**Figure 2**). Collectively, these data suggested that PI3K/AKT/mTOR/MEK play important roles in the progression of tumors and serve as a reliable biomarker of poor prognosis.

PPI enrichment of PI3K/AKT/mTOR/MEK signature

To gain insight into the patterns of the effects of the PI3K/AKT/mTOR and MEK clustering network on the biological processes in cancer, the enrichment analysis was performed to identify the pathways involved in the signature. We obtained several biologically sensible themes enriched in the signature, which proved that the PI3K/AKT/mTOR and MEK were mainly involved in metabolism and cancer activation (Supplementary Figure 1). Metabolic disorders are a key event in the development of cancer, and it constitutes one of the signs of cancer [61]. KEGG pathway analysis revealed that the signature was highly enriched in type II diabetes mellitus, central carbon metabolism in cancer, acute myeloid leukemia, adipocytokine signaling pathway, pancreatic cancer, glioma, ErbB signaling pathway colorectal cancer, prostate cancer, choline metabolism in cancer. In accordance with our observations, previous studies have identified these gene signature as cancer-associated genes. For instance, Murugan et al. [62] reported that mTOR promotes cancer growth, drug resistance, and metastasis, while McCubrey et al. [63] reported that the EGFR/mTOR signaling pathways play prominent roles in malignant transformation, therapeutic resistance, cancer stemness, metastasis, and inhibition of apoptosis. MAP2K was implicated in hypoxia-mediated angiogenesis, cancer progression, metastasis, and drug resistance [64]. Collectively, these results confirmed the oncogenic roles of PI3K/AKT/mTOR/MEK signature signatures in multiple cancers.

PI3K/AKT/mTOR-MEK expressions are associated with tumor immune infiltrations

The immunotherapeutic response can vary widely among patients receiving the same treatment for the disease of the same stage [65]. Tissue immune infiltration is highly involved in immune reactions [66], and Immunotherapy is currently a routine cancer treatment option. Therefore, we queried the associations of PI3K/AKT/mTOR-MEK expressions with infiltrations of various tumor immune cells in multiple cancers. Our results revealed that mTOR expression was strongly correlated (all $r > 0.3$, $P < 0.03$) with the infiltrations of $CD4^+$ T Cell, neutrophil, and dendritic Cell in COAD; $CD4^+$ T Cell infiltration in HNSC; and, neutrophil infiltration in LIHC and SKCM. Week correlation (all r $0.1 \sim \leq 0.3$, $P < 0.005$) with infiltration of $CD8^+$ T Cell, and neutrophil in BRCA; $CD4^+$ T Cell in GBM; neutrophil and dendritic cell in HNSC; $CD4^+$ T Cell and neutrophil in LIHC; neutrophil in LUAD; and, $CD8^+$ T Cell and dendritic cell infiltration in SKCM. In addition, B Cell, $CD8^+$ T Cell, and macrophages infiltration show a negative correlation with mTOR expression (Supplementary Figure 2). For AKT, we observed a strong positive correlation with $CD4^+$ T Cell infiltrations in LICH, COAD, HNSC, and LUAD, while $CD8^+$ T Cell correlates negatively with AKT expressions in HNSC and LUAD (Supplementary Figure 3; Supplementary Table 1).

These results are very relevant in planning immunotherapeutic strategies. $CD8^+$ cytotoxic T lymphocytes recognize MHC I-presenting antigens and are preferred for targeting tumor cells. $CD4^+$ T lymphocytes, on the other hand, play complex and crucial roles in tumor immunity [67]. $CD4^+$ T cells are known to inhibit the cytotoxic properties of $CD8^+$ T lymphocytes, promote metastasis, and are associated with poor prognosis of cancer patients [68]. A previous study revealed that gene-driven oncogenesis of cancer established an immunosuppressive microenvironment via recruitment and activity of $CD4^+$ T lymphocytes [69]. The $CD4^+$ T lymphocytes subsets that play the immunosuppressive roles remain to be elucidated. Certain $CD4^+$ T lymphocytes subsets may also be essential for antitumor immunity. $CD4^+$ helper T cells may promote and maintain cytotoxic T lymphocyte (CTL) memory, amplify T- and B cells, and help CTL overcome negative regulation [70]. $CD4^+$ T lymphocytes may eliminate tumor cells by cytolysis or by regulating the tumor microenvironment [71]. More detailed studies are therefore required to elucidate the infiltration and specific role of each $CD4^+$ T lymphocyte subset in immunotherapy. Collectively, our findings suggest that, considering the differential infiltration level of $CD8^+$ T Cell and $CD8^+$ T Cell in cohorts expressing high AKT and mTOR, patients expressing a high level of this signature may benefit from more accurate immunotherapy strategies and could facilitate the measurement of immunotherapeutic response. In addition, this finding suggests that targeting AKT and mTOR will be an excellent addition to immunotherapy in multiple cancers.

At present, in addition to immune checkpoint inhibitors, more drugs, such as mTOR inhibitors are widely applied [72] and becoming current

and emerging therapeutic options [73]. Therefore, the mTOR-targeting small molecule reported in this study could be of immunotherapeutic relevance for future clinical drug research. MET and PIK3CA expression also shows strong (all r 0.3~0.4, $P < 0.005$) or very strong correlations (all $r > 0.4$, $P < 0.005$) with infiltration of various immune cells in various cancers (Supplementary Figures 4 and 5). It is, however, noteworthy that MET expression correlates negatively with all immune cell infiltrations in GBM excepting the $CD4^+$ T Cell and dendritic cell infiltrations, while PIK3CA expression shows a week (all $r \leq 0.09$, $P < 0.005$) or negative correlation with various immune cell infiltrations in HNSC and GBM (all $r \leq -0.00$, $P < 0.005$), suggesting that these genes signature are poor prognosticator of glioma immune infiltration and could not be used in the measurement of immunotherapy response in glioblastoma. However, further experimental studies are needed for accurate and reliable applications in the clinic.

PI3K/AKT/mTOR-MEK expressions are associated with CAF infiltrations

mTOR expression shows a positive correlation with CAF infiltrations in the various cancer types except for the low-grade glioma ($r = -0.02749$). Particularly, a very strong positive correlation ($r > 0.5$, $P < 0.05$) was observed for CHOL and PAAD (**Figure 1**). Similarly, PIK3CA show a very strong correlation (all $r > 0.5$) with CAF infiltration in READ, PAAD, COAD, and CHOL, but low to strong correlation ($r = 0.01$ to ≤ 4.0) with CAF infiltrations in other cancers, excepting the LGG ($r = -0.05387$). AKT expressions also correlated with CAF infiltrations in all the cancer types excepting THCA, KIRP, BRCA-Her2, and KICH, while MEK expressions show low to strong correlation ($r \geq 0.1$ to > 4.0) with CAF infiltrations in various cancers excepting TGCT ($r = -0.15464$), PRAD ($r = 0.083965$), LGG ($r = 0.066395$) and BRCA-LumB ($r = -0.08549$) (Supplementary Figure 6A; Supplementary Table 2). In order to evaluate the prognostic relevance of these associations, we classified the cohorts into 4 groups; ^{low}CAF + ^{low}PI3K/AKT/mTOR-MEK, ^{low}CAF + ^{high}PI3K/AKT/mTOR-MEK, ^{high}CAF + ^{low}PI3K/AKT/mTOR-MEK, and ^{high}CAF + ^{high}PI3K/AKT/mTOR-MEK. Remarkably, we found that the cohorts in ^{low}CAF + ^{low}PI3K/AKT/mTOR-MEK exhibited longer cumulative survival while cohorts of ^{high}CAF + ^{high}PI3K/AKT/mTOR-MEK had the shortest cumulative survival (Supplementary Figure 6B).

Rationale for NSC777213 design and its biological activity mapping

Although major advances have been made in the chemotherapeutic management of patients with cancer [74], cancer remains the major global health problem partially due to drug resistance and the adverse effects of conventional therapies. In this study, we present a new small molecule containing a 3-(2-fluoro-4-iodophenyl)-substituent and isoflavone core as PI3K/AKT/mTOR-MEK inhibitors. Our ligand was designed based on structural evaluation and a previous quantitate structure activity relationship (QSAR) analysis of MEK inhibitors. We observed that majority of MEK inhibitors in clinical development, including pimasertib, refametinib, cobimetinib (GDC0973), mirdametinib (PD0325901) (phase I), and TAK733 (phase I), share a similar substituted 2-fluoro-4-iodophenyl moiety (**Figure 3A**). Furthermore, the QSAR analysis indicated the importance of 2-fluoro-4-iodoaniline motif in MEK inhibitor activity [75]. To this end, we employ a fragment based drug design and molecular hybridization strategy to developed NSC777213 based on the assumption that the 2-fluoro-4-iodophenyl moiety of clinical MEK inhibitor can form a new hydrogen bond with the isoflavone backbone (**Figure 3B**).

Following the synthesis of NSC777213 as we earlier reported [76], we predicted it possible biological activity by using PASS software, an online algorithm designed for evaluating the general biological properties of drug-like small molecules based on their structure [77]. We found that the major biological activities (all pa > pi) of NSC777213 were antineoplastic effects against pancreatic, colorectal, and breast cancer, glioblastoma multiforme, and non-Hodgkin's lymphoma. Other biological activities of NSC777213 include the treatment of inflammatory, hepatorenal, neurodegenerative, autoimmune disorder, pains and microbial infection (Supplementary Table 3). These findings suggest that NSC777213 is a promising bioactive compound with a broad spectrum of biological activity. However, in this study, we chose to focus on assessing its anticancer activity *in vitro* by using the well characterized standard NCI60 panels of human tumor cell lines.

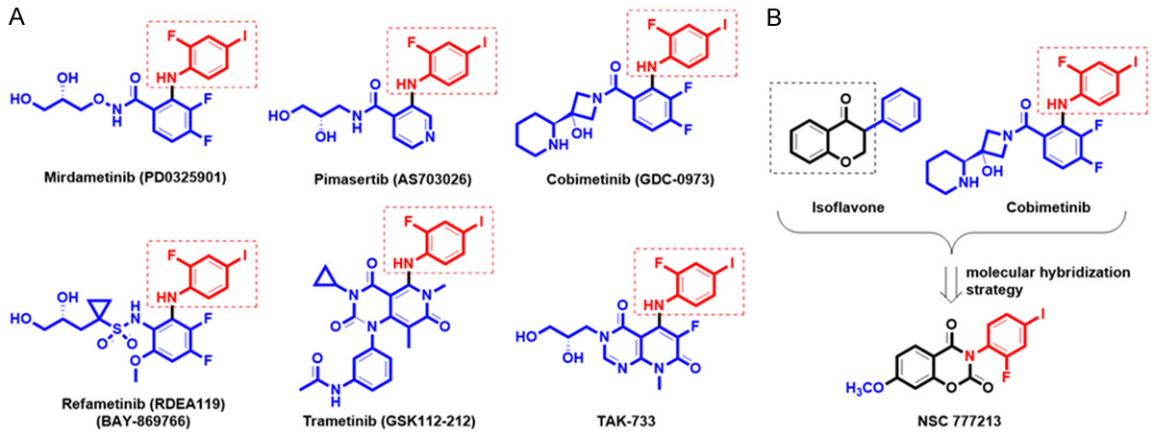

Figure 3. NSC777213 design strategies. A. The chemical structures of 5 representatives of MEK inhibitors in clinical development. These clinical inhibitors share similar aniline (2-fluoro-4-iodophenyl) group. B. Schematic representation of NSC777213 design via fragment-based drug design and molecular hybridization of isoflavone and aniline (2-fluoro-4-iodophenyl) moiety of cobimetinib.

NSC777213 exhibited antiproliferative activities against the NCI60 panels of human tumor cell lines

In recent decades, more research has been conducted on small-molecule anticancer agents due to their effectiveness and selective multitarget properties [78]. In this study, using the well characterized NCI60 human tumor cell line panel, we demonstrated the anticancer activities of NSC777213. At an initial, single-dose (10 μM) screening, NSC777213 demonstrated an antiproliferative effect against the cell line panels of breast, prostate, renal, ovarian, colon, and central nervous system (CNS) cancer; NSCLC; melanoma; and leukemia. Except for the ovarian cancer cell line (OVCAR-5) and colon cancer cell lines (COLO205 and HT29), more than 70% growth was inhibited by NSC777213 in all the cell line panels (**Figure 4**). Furthermore, a single dose of NSC777213 exhibited a pronounced lethal effect on the cell line panels of NSCLC (HOP-92 [GI = -23.13%], NCI-H23 [GI = -4.02%], NCI-H522 [GI = -11.29%]), melanoma (MALME-3M [GI = -5.22%], SK-MEL-2 [GI = -20.09%], and SK-MEL-5 [GI = -63.97%]), and renal cancer (A498 [GI = -20.85%] and UO-31 [GI = -3.22%]). The trend of these single-dose anticancer screening results of NSC777213 is in line with those of the anticancer activities of structurally related small molecules (NSC765599 and NSC765690), as reported in a recent finding [50]. Collectively, these findings clearly indicate the antiproliferative activities of NSC777213 against various human cancer cell lines and, thus, formed the basis for its evaluation in our dose-dependent assay.

NSC777213 exhibited dose-dependent anticancer activities and cytotoxic preference for NSCLC, melanoma, and CNS and renal cancer cell lines

NSC777213 exhibited dose dependent anticancer activities on the cell line panels (**Figure 5**). In agreement with the results for single-dose screening, NSC777213 demonstrated high inhibitory activities (GI_{50} = 0.38-6.02 μM) against all the panels of NCI60 human tumor cell lines, except COLO205 (GI_{50} = 14.10 μM) and HT29 (GI_{50} = 25.90 μM). The most responsive cell line panels were those of ovarian cancer (GI_{50} = 2.41-2.98 μM), melanoma (GI_{50} = 0.42-3.47 μM), leukemia (GI_{50} = 1.01-3.16 μM), and NSCLC (GI_{50} = 0.38-3.77 μM). In addition, the TGI and LC_{50} concentrations indicated that the cell lines of leukemia (RPMI-8226 and HL-60(TB), NSCLC (HOP-92 and HOP-62), CNS cancer (SF-295, SNB-75, and U251), breast cancer (MDA-MB-468, T-47D, and MCF7), and melanoma (MALME-3M, SK-MEL-2, SK-MEL-5, UACC-257, and UACC-62) were the most responsive to the anticancer activities of NSC777213, whereas prostate, ovarian, and colon cancer cell lines demonstrated some degree of cytotoxic resistance to NSC777213 (**Figure 6**). Surprisingly, the chemoresistant ovarian cancer cell lines, including SK-OV-3 (TGI = 7.62) OVCAR-3 (TGI = 9.23), OVCAR-4 (TGI = 31.50),

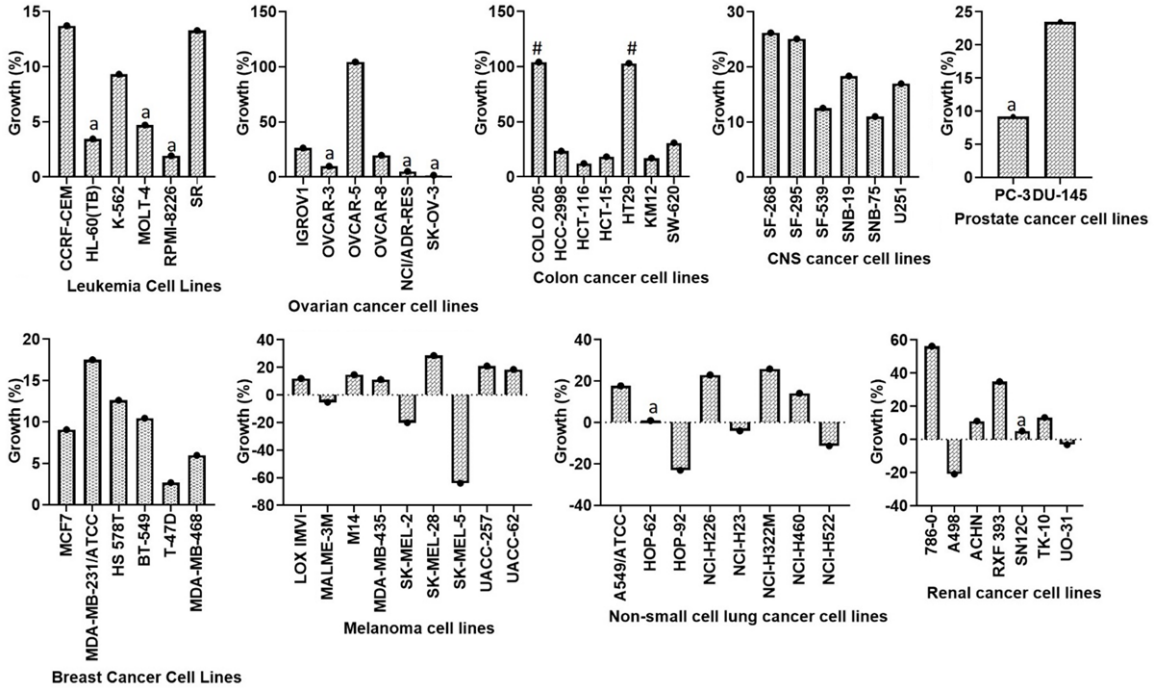

Figure 4. Anti-proliferative effect of NSC777213 against the NCI60 panels of human cancer cell lines. Each cell line was treated with a single dose of (10 μM) of NSC777213. The zero points indicate the mean cell growth. The percentage growth inhibition of each cell line relative to the mean is represented by values under 100, whereas those values below 0 designate cell death. Bars with "a" superscript represent cell lines with more than 90% cell growth inhibition, while "#" cell resistance (no growth inhibition).

and NCI/ADR-RES (TGI = 10.20), exhibited higher sensitivity to NSC777213 than did the parental cell lines, OVCAR-8 and IGROV1 (TGI > 100). SK-OV-3 was established from the malignant ascites of a patient with drug-resistant ovarian adenocarcinoma after combination chemotherapy with cyclophosphamide, adriamycin, and cisplatin [79], whereas SK-OV-3, OVCAR-4, and NCI/ADR-RES are genetically well profiled and known to be resistant to multiple clinical drugs [80, 81]. In addition, NSC777213 exhibited a high cytotoxic effect (TG1 = 28.1 μM and LC_{50} = 55.60 μM) against COLO205 despite its resistance to single-dose treatment. This finding accords with that in a previous study that EBI-1051, a novel small molecule that was designed using a similar approach with our NSC777213, exhibited good activity against the MEK1 enzyme (IC_{50} = 7.0 nM) and COLO205 cell line (IC_{50} = 7.2 nM) [75]. COLO205 was derived from patients with colon cancer following therapeutic failure of 5-fluorouracil. Therefore, the study results suggest that NSC777213 is useful in treating drug-resistant cancers, particularly chemotherapy-resistant ovarian cancers. Collectively, the findings from the anticancer screening of NSC777213 indicated its antiproliferative activities against all panels of NCI60 human tumor cell lines, except COLO205 and HT29. However, NSC777213 is not generally toxic to growing cell lines but exhibits selective cytotoxic preference for NSCLC; melanoma; and CNS, renal, and ovarian cancer cell lines. Our study suggests that NSC777213 is a promising candidate for further preclinical and clinical evaluation as a chemotherapeutic agent, particularly to treat NSCLC; melanoma; and brain, renal, and ovarian cancer.

NSC765599 anticancer fingerprints are mechanistically correlated with NCI inhibitors of PI3K/AKT/mTOR signaling pathways

To facilitate the rapid identification of the molecular mechanism of anticancer agents, NCI60 cell lines have been well characterized for mutation and genetic and protein expression patterns, and a computational tool, DTP-COMPARE algorithm, was developed to identify the mechanism(s) of action and molecular targets of anticancer compounds based on the similarity of its anticancer fingerprints to that of known compounds and the molecular profile of the cell lines [82]. In the present study, NCI's

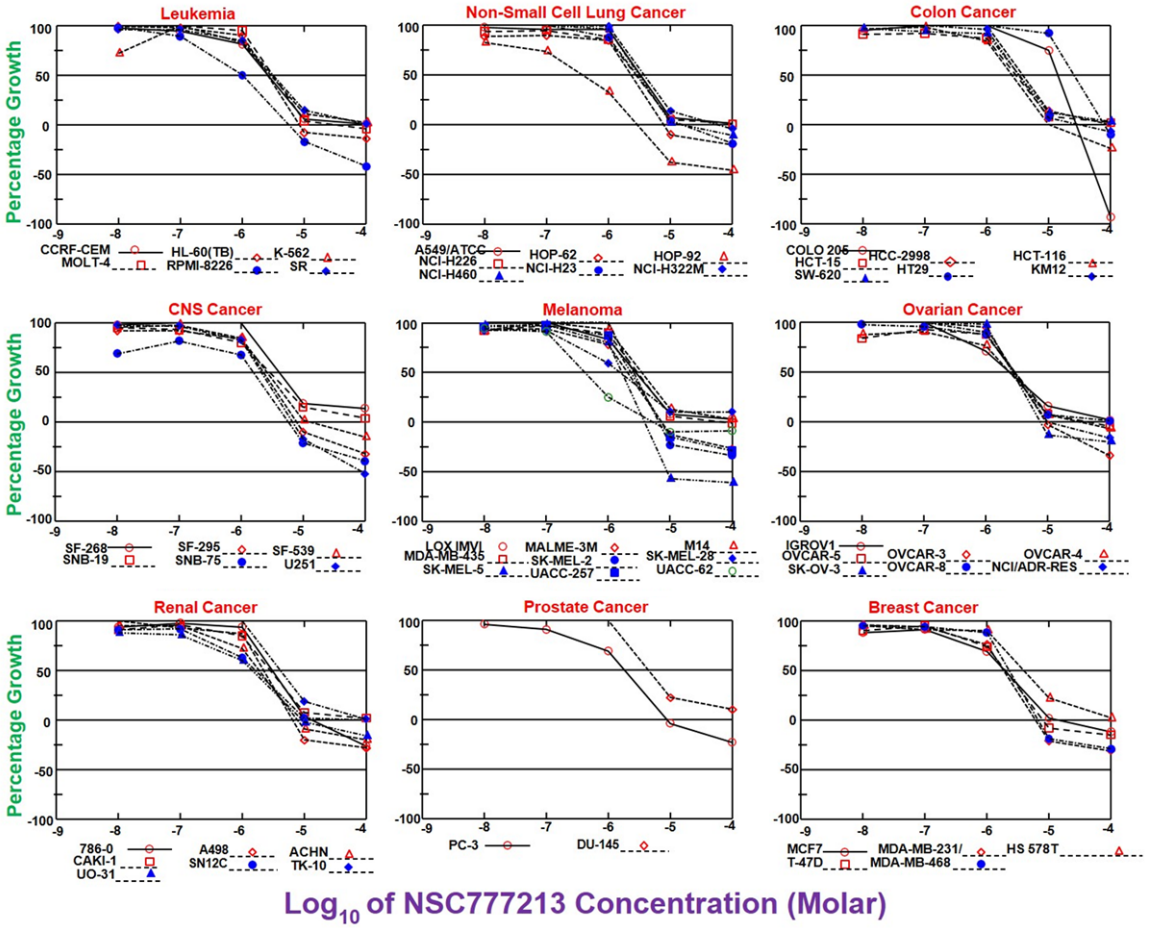

Figure 5. Dose-dependent response curves of NSC777213 against NCI60 panels of human tumor cell lines. On the Y-axis, the percentage growth value of +100 represents growth of non-treated cells, the 0 value indicate no net growth, while the value under 0 represents cell death.

COMPARE algorithm results indicated that NSC777213 anticancer activity correlates with the anticancer fingerprints of some NCI investigational, mechanistic and marketed drugs (**Table 1**). Particularly, we observed a correlation with numerous known inhibitors of PI3K/AKT/mTOR and MEK signaling pathways, including copanlisib (P = 0.25, CCLC = 56), vandetanib (P = 0.27, CCLC = 54), idelalisib (P = 0.19, CCLC = 55), temsirolimus (P = 0.14, CCLC = 54), trametinib (P = 0.32, CCLC = 56), and cobimetinib (P = 0.28, CCLC = 56). The 10 NCI synthetic compounds that are mostly correlated with NSC777213 anticancer fingerprints (*p*-value range of 0.61-0.71, CCLC = 44-56) are small molecules with molecular weight ranging between 308.4 and 538.5 g/mol (**Table 2**). The most correlated (*p* value = 0.40-0.63, CCLC = 44-52) mechanistic agents are dominated by natural antimicrobial and anticancer products (such as those from bacteria, fungi, and plants). Importantly, NSC777213 exhibits a strong correlation (*p* value = 0.4-0.7, CCLC = 53-56) with numerous PI3K/AKT/mTOR inhibitors (CC115, GDC0349, AZD3147, AZD5363, MTX211, voxtalisib, and BKM120) currently under detailed investigation by the NCI. Furthermore, other investigational drugs, including the inhibitors of Wnt/B-catenin, PTEFb/CDK9, and IGF-1R, exhibit a strong correlation with the anticancer fingerprints of NSC777213. In addition, the DTP-COMPARE molecular target analysis revealed that the NSC777213 anticancer fingerprint correlated with the expression fingerprints of multiple genes. Among the top molecular targets, the most common correlated fingerprints using TGI, TIG, and LC_{50} as endpoints are FGF3, AKT, RPS6KB1, PIK3R2, PIK3CB, PIK3CA, CCNB1, MET, AKT, and EGFR (**Table 3**). Collectively this study indicated that the anticancer and molec-

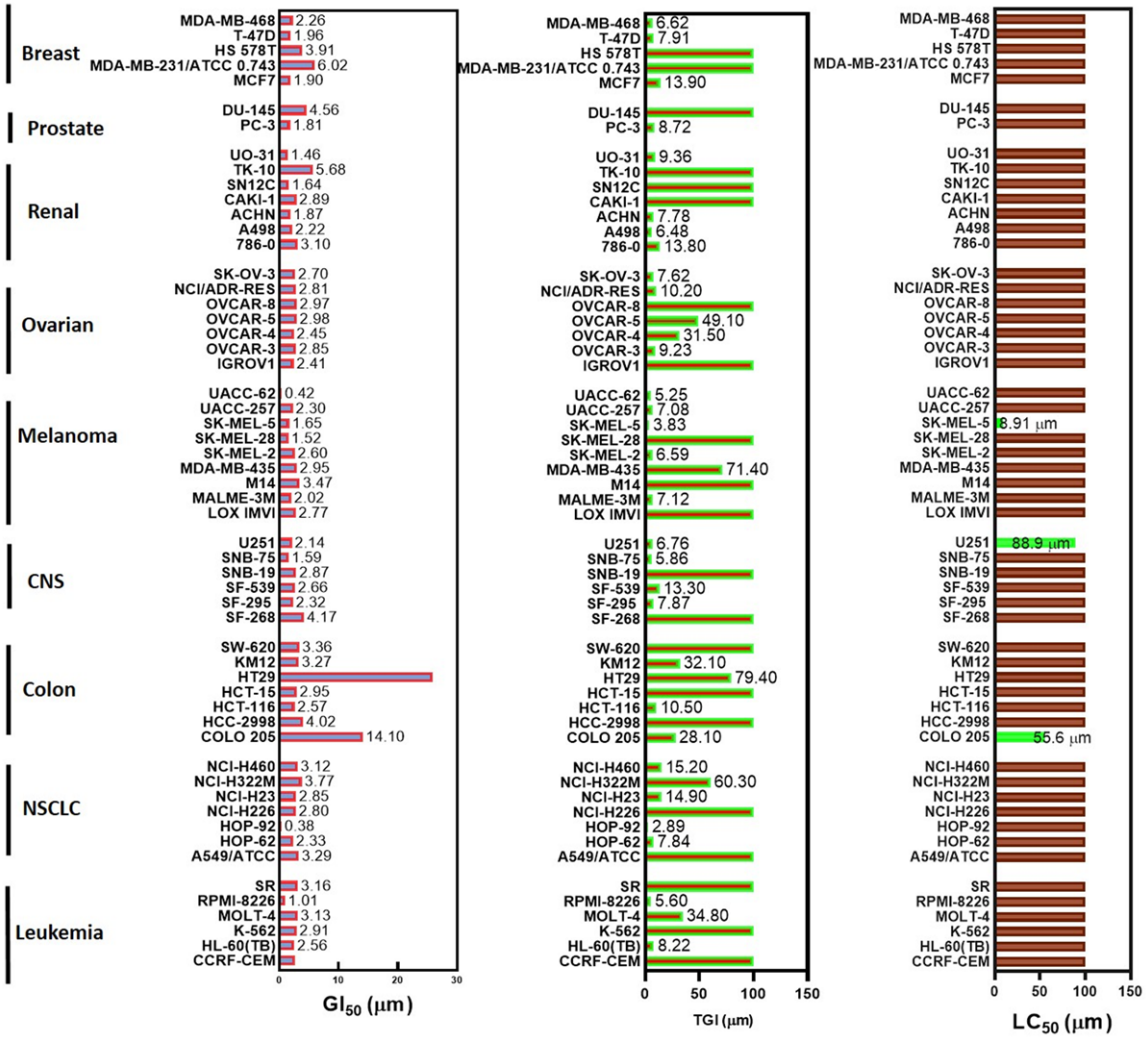

Figure 6. Anti-proliferative and cytotoxic activities of NSC777213 against f NCI60 panels of human tumor cell lines. The GI_{50} = 50% growth inhibition, TGI = total growth inhibition, LC_{50} = 50% loss of cells.

ular target fingerprints of NSC777213 correlated well with PI3K/AKT/mTOR and MEK signaling pathways and, hence, provided strong evidence that targeting PI3K/AKT/mTOR and MEK is the most probable mechanism of action of NSC777213. These molecular targets should be considered as the first priority and should be explored for hit-to-lead optimization by using further in silico and in vitro studies [83].

NSC777213 has potential target preference for protein regulators of cell cycle and PI3K/AKT/mTOR signaling pathways

In silico methods have immensely contributed to drug target identification and the rational guidance of the processes of drug discovery [84, 85]. We used the SwissTargetPrediction algorithm to identify the most probable macromolecular targets of NSC777213 on the basis of similarity with a known active compound in the library [86] and found that kinases are the major targets for NSC777213. Interestingly, the protein kinases, serine/threonine-protein kinase mTOR, PI3-kinase p110-delta/p85-alpha, PI3-kinase p110-alpha, delta and gamma subunit, MAP kinase ERK1/2, and serine/threonine-protein kinase Chk1 are among the top-ranked targets (**Table 4**). Furthermore, using the PharmMapper algorithm, an integrated pharmacophore-matching server with statistical modules for identifying potential drug targets, 5 members of MAP kinases (normalized score > 0.9 and z-score > 0.5), PIK3CA (normal-

Table 1. NCI-investigational, mechanistic and marketed anticancer drug sharing similar anti-cancer fingerprints and mechanistic correlation with NSC777213

s/no	p	CCLC	Target-NSC	Market drug	Target Description
1	0.41	49	3053	actinomycin D	Transcription inhibitor
2	0.32	56	758246	Trametinib	MEK inhibitor
3	0.31	54	755980	Lenvatinib	VEGFR inhibitor
4	0.28	56	768068	Cobimetinib	MEK inhibitor
5	0.27	54	760766	Vandetanib	EGFR inhibitor
6	0.25	54	763932	Regorafenib	Kinase inhibitor
7	0.25	56	760443	Copanlisib	PI3K inhibitor
8	0.19	55	759224	Idelalisib	PI3K inhibitor
9	0.15	56	779217	Osimertinib	EGFR inhibitor
10	0.14	54	683864	Temsirolimus	mTOR inhibitor
	P	CCLC	Target-NSC	Mechanistic agent	Description
1	0.63	44	241906	Uvaretin	Flavonoid
2	0.49	44	24817	Peltatin A	phenols
3	0.48	44	10447	Purpurin	quinone
4	0.45	44	243023	Cinerubin B Hydrochloride	Streptomyces sp.
5	0.41	44	285223	Neothramycin	Streptomyces
6	0.41	44	65104	Septacidin	Streptomyces
7	0.41	49	3053	Actinomycin D	Bacteria
8	0.41	52	352890	9-Deazaadenosine	Synthectic
9	0.4	49	107067	Tirandamycin	Natural Product
10	0.4	44	265450	Nogalomycin C	Bacteria
	P	CCLC	Target-NSC	Investigational Drug	Activity
1	0.70	56	778746	FH535	Wnt/B-catenin
2	0.53	56	793151	CC115	mTOR kinase inhibitor
3	0.51	50	786098	BAY1143572	PTEFb/CDK9 inhibitor
4	0.48	56	764582	10058-F4	c-Myc inhibitor
5	0.46	56	780042	CP-724714	rbB2 (HER2) tyrosine kinase inhibitor
6	0.44	56	771532	GDC-0349	mTOR/PI3K inhibitor,
7	0.42	56	784815	AZD-3147	mTORC1 and Mtorc2 inhibitor
8	0.42	56	756652	LINSITINIB	IGF-1R inhibitor
9	0.41	56	764039	AZD-5363	Inhibitor of all AKT isoforms
10	0.41	56	803248	MTX211	EGFR and PI3K inhibitor
11	0.40	55	791226	Voxtalisib	PI3K/mTOR Inhibitor
12	0.40	53	800892	EVOBRUTINIB	BTK inhibitor
13	0.40	55	784722	INNO-206	DNA topoisomerase II inhibitor
14	0.40	56	754353	BKM-120 (PI3K)	Inhibitor of PI3K isoform α (PIK3CA)
15	0.40	56	762153	ST-3595	HDAC inhibitor

P: Pearson's correlation coefficient. CCLC: Common cell lines count.

ized score = 0.7863), 3-phosphoinositide-dependent protein kinase 1 (normalized fit = 0.763), and 3 members of the serine/threonine-protein kinases (normalized fit = > 0.5) were identified as the major NSC777213 targets (Supplementary Table 4). The model further revealed 3 hydrophobic interactions between NSC777213 and MEK (normalized fit score of 0.9909 and z-score of 1.04924) and, 2 hydrophobic as well as 1 hydrogen acceptor interactions between NSC777213 PIK3CA (**Figure 7**). Thus, in accordance with our expectations, NCI-COMPARE analysis together with various in silico algorithms collectively identified PI3K/AKT/mTOR and MEK pathways as the most probable targets for NSC777213. Thus,

Table 2. NCI-synthetic anticancer drug sharing similar anti-cancer fingerprints with NSC777213

s/n	p	CCLC	Target NSC	MW (g/moL)	Synthetic compound
1	0.71	55	777205		3-(4-chloro-2-fluorophenyl)-2H-benzo[e[1,3]oxazine-2,4(3H)-dione
2	0.7	56	778746	361.2	2,5-dichloro-N-(2-methyl-4-nitrophenyl)benzenesulfonamide
3	0.69	55	777207		3-(4-chloro-2-fluorophenyl)-7-methoxy-2H-benzo[e][1,3]oxazine-2,4(3H)-dione
4	0.67	55	766728	401.9	N-[(4-chlorophenyl)-(2-hydroxynaphthalen-1-yl)methyl]-2-phenylacetamide
5	0.64	53	775790	510.1	[4,5-dichloro-1-[4,5-dichloro-2-(2-hydroxybenzoyl)-1H-pyrrol-3-yl]pyrrol-2-yl]-(2-hydroxyphenyl)methanone
6	0.64	44	208915	308.4	ethyl 2-[1-adamantylcarbamoyl(ethyl)amino]acetate
7	0.63	44	241906	378.4	1-[2,4-dihydroxy-3-[(2-hydroxyphenyl)methyl]-6-methoxyphenyl]-3-phenylpropan-1-one
8	0.62	56	103073	450.8	3-N-[(Z)-[4-[bis(2-chloroethyl)amino]-5-ethoxy-2-methylphenyl]methylideneamino]-5-methyl-1,2,4-triazole-3,4-diamine;hydrochloride
	0.61	47	328477	306.0	N-(3-chloro-2-methylphenyl)-2-hydroxy-3-nitrobenzamide
9	0.61	47	601617	538.5	1',3'-dihydroxy-6'-methoxy-1,4',5',8',9'-pentaoxo-3-[(1E,3E)-penta-1,3-dienyl]spiro[6,7-dihydro-2H-cyclopenta[g]isoquinoline-8,2'-cyclopenta[b]naphthalene]-9-olate
10	0.61	56	27102	384.13	2-hydroxy-N-(4-iodophenyl)-3-nitrobenzamide

P: Pearson's correlation coefficient. CCLC: Common cell lines count. MW: molecular weight.

Table 3. Molecular targets correlated to NSC777213 Anticancer fingerprint

#	LC_{50} Endpoint			TGI Endpoint			GI_{50} Endpoint		
	p	CCL	NCI Target	p	CCL	NCI Target	p	CCL	NCI Target
1	0.42	50	IGHMBP2	0.24	55	PIK3CA	0.25	50	RARB
2	0.36	54	CTTN	0.21	50	RAB2	0.23	51	PIK3R2
3	0.30	55	FGF3	0.18	54	CTTN	0.22	55	MYCN
4	0.30	55	BRCA2	0.18	55	DBF4B	0.19	54	RAF1
5	0.29	55	CCND1	0.17	54	STAG1	0.18	54	CACNA1D
6	0.24	55	AKT1	0.17	55	PIK3CB	0.15	54	S100B
7	0.22	52	SLC20A2	0.17	48	FGFR1	0.14	55	PIK3CB
8	0.20	55	MYB	0.16	55	RPS6KB1	0.12	55	EGFR
9	0.18	55	RPS6KB1	0.16	54	TGFB2	0.11	55	RPS6KB1
10	0.13	55	MET	0.12	54	AKT1	0.11	54	AKT1
11	0.13	55	MET	0.12	51	PIK3R2	0.11	52	CCNB1

P: Pearson's correlation coefficient. CCLC: Common cell lines count.

they were further validated using a structural simulation of protein-ligand interactions.

Molecular docking revealed a robust Interaction of NSC777213 with PI3K/AKT/mTOR-MEK

Molecular docking has become an increasingly valuable tool in the early stage of drug discovery and development [87]. It is used to model the interaction between a small-molecule drug candidate and a protein target at the atomic level, allowing for the depiction of small-molecule behavior at the binding site of target proteins and elucidating possible fundamental biochemical processes regulated by the small molecule [88, 89]. In this study, the molecular docking analysis indicated that NSC765599 docked well into the binding cavity of P13K/AKT/mTOR/MEK (**Figures 8-11**). Hydrogen bonds as well as other noncovalent interactions, such as hydrophobic and ionic interactions and Van der Waals forces, play crucial roles in stabilizing the interaction between small molecules and protein targets [90]. We found that NSC777213 interactions with P13K/AKT/mTOR/MEK predominantly involved hydrogen bonds, Van der Waals forces, and various π-interactions (**Tables 5** and **6**), having high interactions and strong binding affinity (ΔG = -8 Kcal/mol, binding distance = 2.39-3.49 Å) to the binding pocket of PI3K (PDB: 3APC) and,

Table 4. SwissTarget prediction of potential NSC777213 targets

Target	Common name	Uniprot ID	ChEMBL ID	Target Class
Serine/threonine-protein kinase mTOR	MTOR	P42345	CHEMBL2842	Kinase
PI3-kinase p110-alpha subunit	PIK3CA	P42336	CHEMBL4005	Enzyme
Cyclin-dependent kinase 5/CDK5 activator 1	CDK5R1 CDK5	Q15078 Q00535	CHEMBL1907600	Kinase
Cyclin-dependent kinase 2	CDK2	P24941	CHEMBL301	Kinase
PI3-kinase p110-delta subunit	PIK3CD	O00329	CHEMBL3130	Enzyme
PI3-kinase p110-gamma subunit	PIK3CG	P48736	CHEMBL3267	Enzyme
Cyclin-dependent kinase 4	CDK4	P11802	CHEMBL331	Kinase
PI3-kinase p110-beta subunit	PIK3CB	P42338	CHEMBL3145	Enzyme
TGF-beta receptor type I	TGFBR1	P36897	CHEMBL4439	Kinase
Cyclin-dependent kinase 1/cyclin B	CCNB3 CDK1 CCNB1 CCNB2	Q8WWL7 P06493 P14635 O95067	CHEMBL2094127	Other cytosolic protein
MAP kinase ERK1/2	MAPK3/1	P27361 P28482	CHEMBL3385	Kinase
PI3-kinase p110-delta/p85-alpha	PIK3CD PIK3R1	O00329 P27986	CHEMBL2111432	Enzyme
Protein kinase C (PKC)	PRKCZ	Q05513	CHEMBL3438	Kinase
Epidermal growth factor receptor erbB1	EGFR	P00533	CHEMBL203	Kinase
Nitric oxide synthase, inducible	NOS2	P35228	CHEMBL4481	Enzyme
Vascular endothelial growth factor receptor 2	KDR	P35968	CHEMBL279	Kinase
Glycogen synthase kinase-3 beta	GSK3B	P49841	CHEMBL262	Kinase
Serine/threonine-protein kinase Chk1, PIM1	CHEK1 PIM1	O14757 P11309	CHEMBL4630 2147	Kinase

Targets were predicted using Swiss Target Prediction, which operates on the principle of 'similarity'.

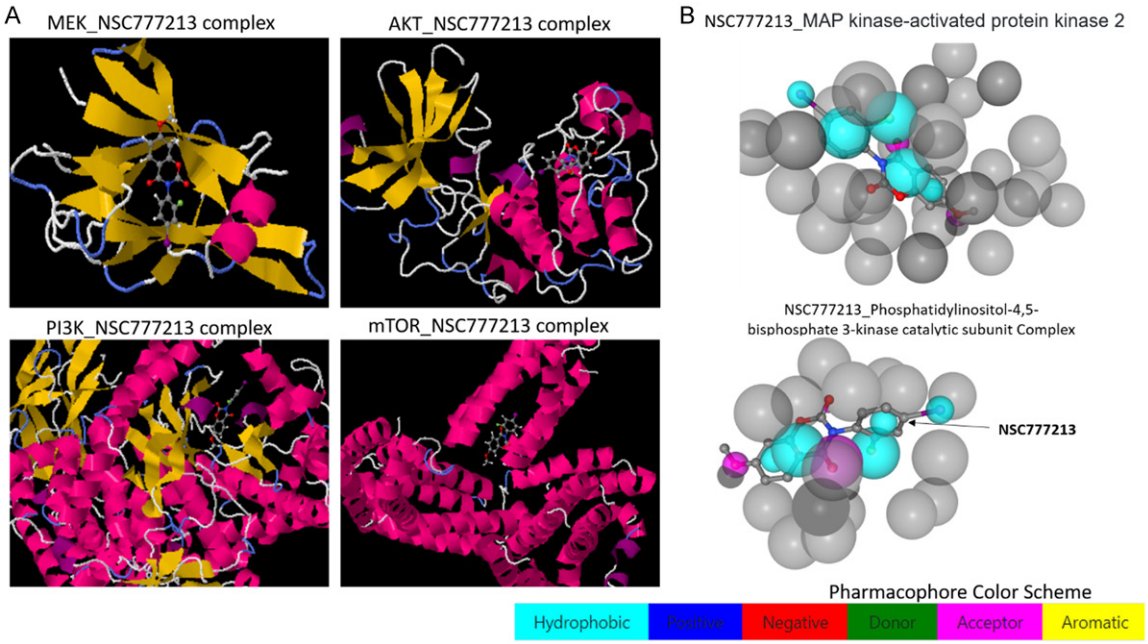

Figure 7. Swissdock and PharmMapper modelled NSC777213 interaction with PI3K/AKT/mTOR/MEK.

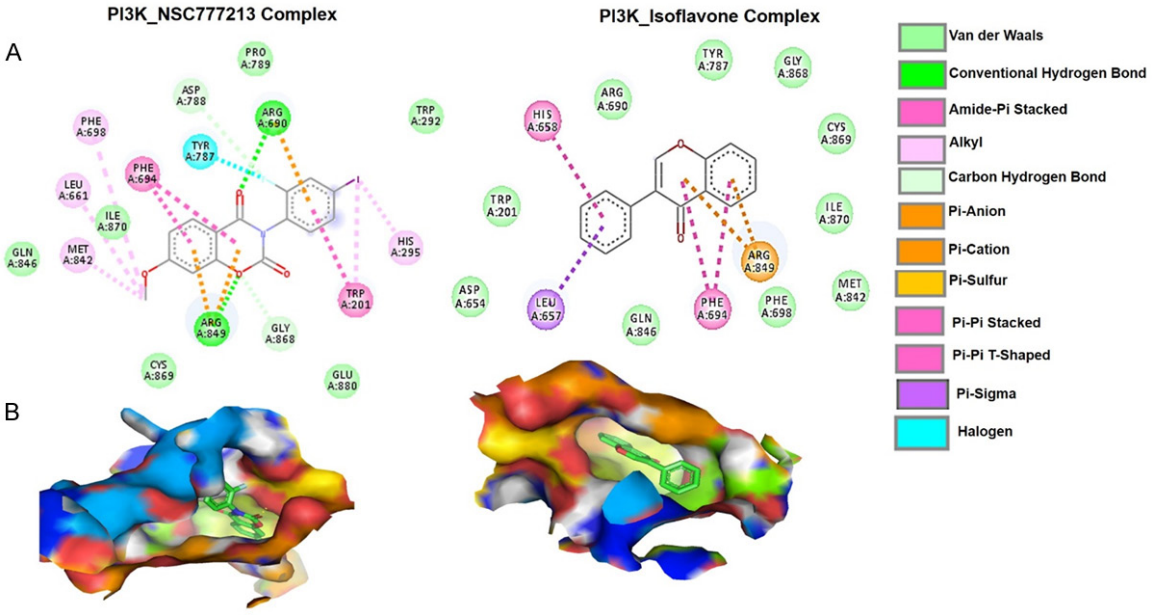

Figure 8. Docking profiles of human PI3K (PDB: 3APC) with NSC777213 and isoflavone. A. The two dimensional (2D) representations of ligand–receptor complexes, showing the interacting amino acid residues and the type of interactions, occurring between the ligands (NSC777213 and isoflavone) and PI3K. B. Solid surface representation of the ligands (NSC777213 and isoflavones) binding-site flap of the PI3K.

thus, represent the most favored receptor for NSC777213 ligandability. Moreover, NSC777-213 interacted with the active site of AKT and mTOR with the affinities of -6.7 and -7.0 kcal/mol, respectively (**Table 5**). An analysis of the interaction revealed that NSC777213 forms a complex with PI3K using 4 H bonds (ARG690, ARG849, GLY868, and ASP788) and halogen interactions with ASP788 and TYR787, where NSC777213_AKT and NSC777213_mTOR co-

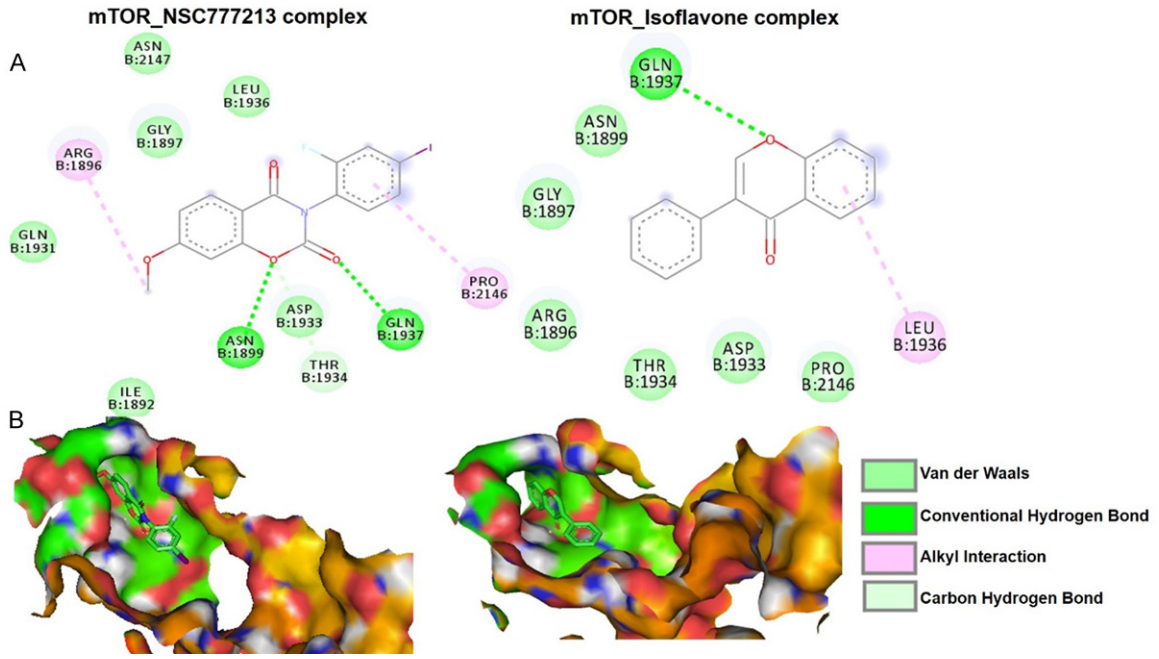

Figure 9. Docking profiles of human mTOR complex 1 (PDB: 5FLC) with NSC777213 and isoflavone. A. The two dimensional (2D) representations of ligand-receptor complexes, showing the interacting amino acid residues and the type of interactions, occurring between the ligands (NSC777213 and isoflavone) and mTOR. B. Solid surface representation of the ligands (NSC777213 and isoflavones) binding-site flap of the mTOR.

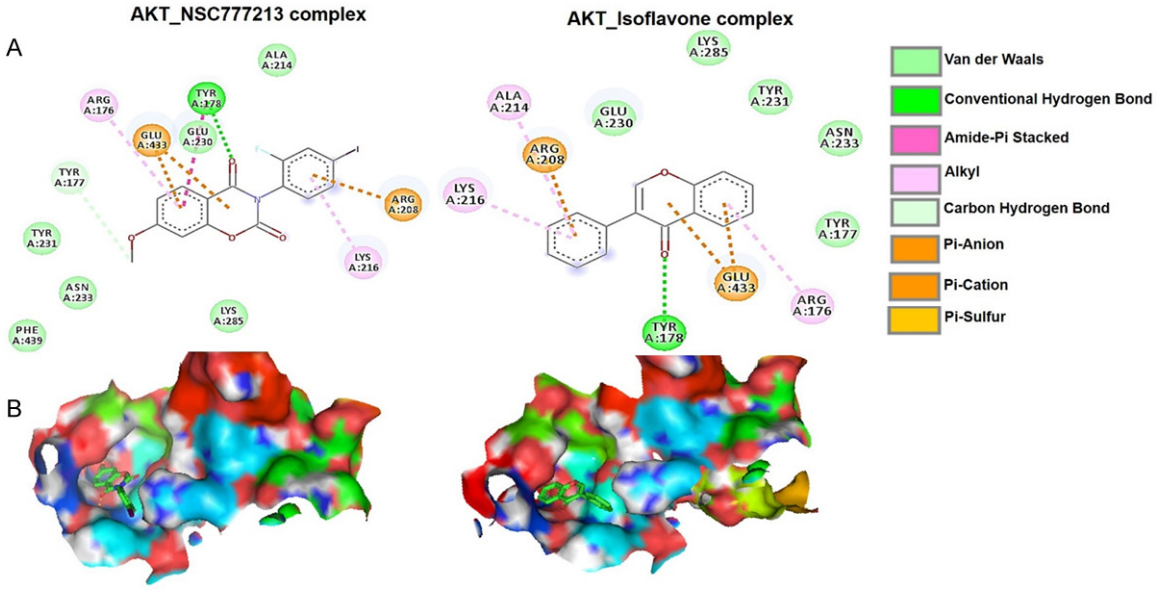

Figure 10. Docking profiles of human AKT kinase domain (PDB: 1GZN) with NSC777213 and isoflavone. A. The two dimensional (2D) representations of ligand–receptor complexes, showing the interacting amino acid residues and the type of interactions, occurring between the ligands (NSC777213 and isoflavone) and AKT. B. Solid surface representation of the ligands (NSC777213 and isoflavones) binding-site flap of the AKT.

mplexes are stabilized by few hydrogen bonds. These high numbers of hydrogens and halogens between NSC777213 and PI3K could be partially responsible for the unique and strong affinity that NSC765690 has for PI3K than it does for AKT/mTOR/MEK (**Tables 5** and **6**).

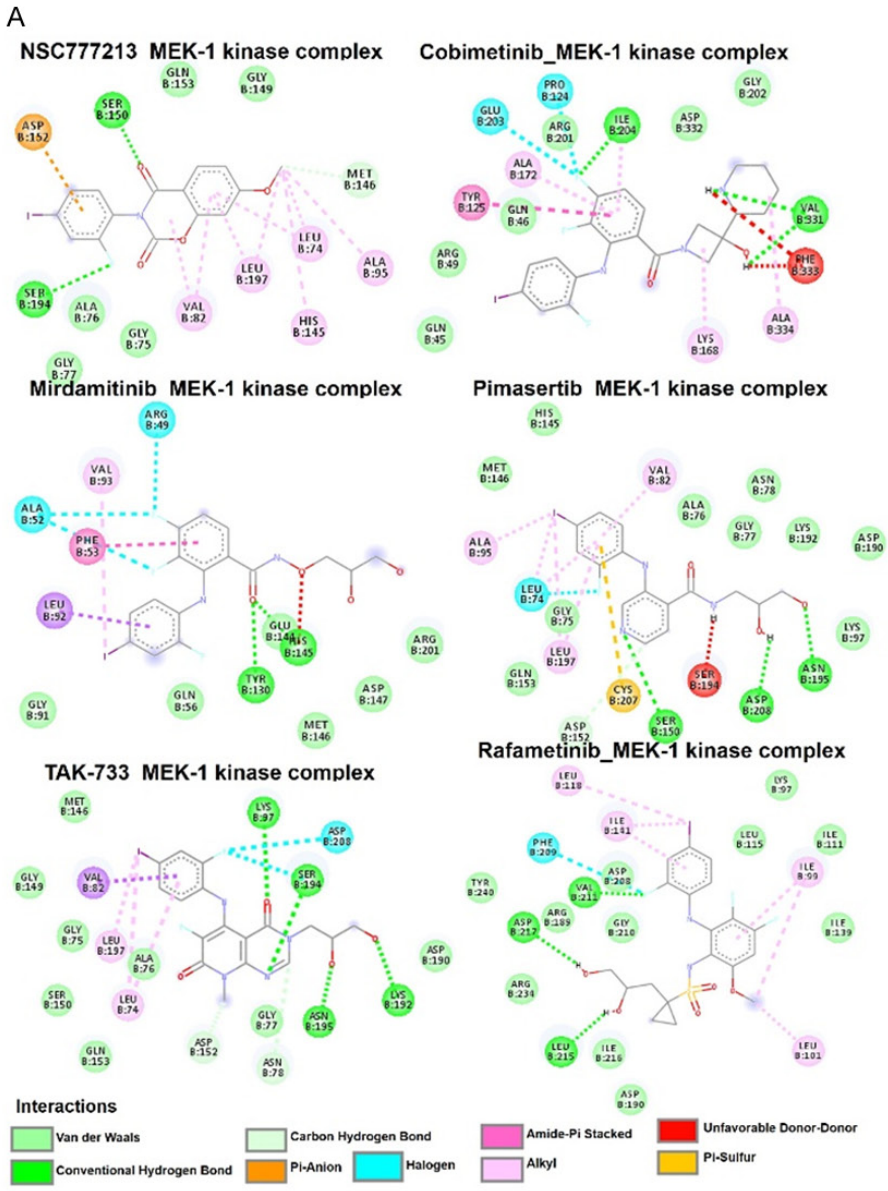

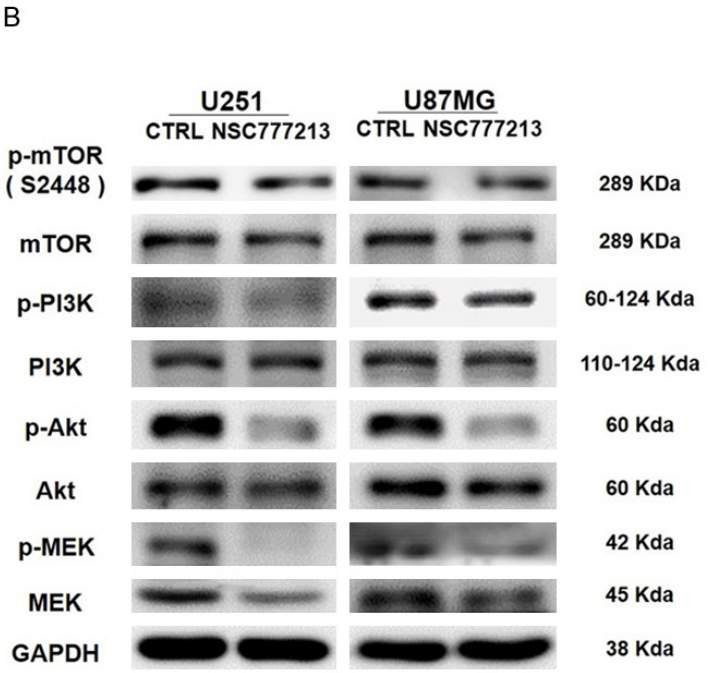

Figure 11. Western blotting, and docking profiles of NSC777213 (A) The two dimensional (2D) representations of ligand-receptor complexes, showing the interacting amino acid residues and the type of interactions, occurring between the ligands (NSC777213 and MEK inhibitors) and MEK-1 kinase (B) Western blots showing that the NSC777213-treated U251 and U87MG cells exhibited lower expression levels of p-mTOR, mTOR, AKT, p-AKT, MEK, p-MEK, P13K and P-PI3K.

Table 5. Comparative docking profile of NSC777213 and isoflavone against PI3K/AKT/mTOR

Interactions	PI3K		AKT		mTOR	
	NSC777213	Isoflavone	NSC777213	Isoflavone	NSC777213	Isoflavone
ΔG = (Kcal/mol)	-8.0	-9.0	-6.7	-6.5	-7.0	-6.8
Conventional H-bond	ARG690 (2.39), ARG849 (3.0)		TYR178 (2.31)	TYR178 (2.57)	GLN1937 (2.51) ASN1899 (2.37)	GLN1937(3.09)
C-H bond	GLY868 (3.49), ASP788 (3.31)		TYR177 (3.66)		THR1934 (3.07)	
Halogen bond	ASP788 (3.23) TYR787 (3.01)					
π-cation	ARG690 (2.39), ARG849 (3.55)	ARG849	ARG208 (3.76)	ARG208 (4.15)		
π-anion			GLU433 (3.37; 4.20)	GLU433 (3.36; 3.81)		
π-alkyl	PHE698, LEU661, MET842, HIS295		ARG176 LYS216	ARG176 LYS216 ALA214	ARG1896 PRO2146	LEU1936
π-π stacked	TRP201	HIS658				
π-π T-shaped	PHE694	PHE694	TYR178			
π-sigma		LEU657				
Van der waal forces	PRO789, TRP292, GLU880, CYS869, GLN846, ILE870	ASP654, TRP201 GLN846, PHE698 MET842, ILE870 CYS869, GLY868 TYR787 ARG690	ALA214, ASN233, TYR231, GLU230, LYS285 PHE439	GLU230, LYS285 TYR231, ASN233 TYR177	GLN1931, ILE1892, ASP1933, SN2147, GLY1897, LEU1936	ASN1899, GLY1897 ARG1896, THR1934 ASP1933, PRO2146

Keys: The values in bracket beside the interacting AA are the binding distance (Å) between the ligand and the corresponding amino acid residues of the receptors.

Table 6. Comparative MEK-1 kinase docking profile between NSC777213 and clinical MEK inhibitors

Interactions	NSC777213	Clinical MEK-inhibitors				
		Cobimetinib	Pimasertib	Mirdametinib	Rafametinib	TAK-733
ΔG = (Kcal/mol)	-7.90	-8.0	-7.60	-6.90	-7.40	-8.60
Conventional H-bond	SER150 (2.31) SER194 (2.93)	ILE204 (1.91) VAL331 (2.14)	ASP208 (1.94) SER150 (2.67) ASN195 (1.92)	HIS145 (2.94) TYR130 (2.06)	VAL211 (2.84) ASP217 (2.24) LEU215 (1.94)	LYS192 (2.13) ASN195 (2.01) SER194 (2.55) LYS97 (2.91)
C-H bond	MET145 (3.66)		ASP152 (3.34)			ASN78 (3.69) ASP152 (3.49)
Halogen bond		GLU203 (3.64) PR0124 (2.99)	LEU74 (3.39)	ALA52 (3.61) ARG49 (3.18)	PHE209 (3.59)	ASP208 (3.62) SER194 (3.48)
π-sulfur			CYS207 (5.73)			
π-alkyl	VAL28, LEU197, HIS145, LEU74, ALA95	ALA172 LYS168 ALA334	ALA95 VAL82 LEU197	VAL93	LEU118 ILE141 ILE99 LEU101	LEU197 LEU74
π-π T-shape		TYR125		PHE53		
π-Anion	ASP152 (4.04)					
Amide-π stacked	LEU74					
Van der waal forces	GLN153, GLY149, ALA76, GLY75 GLY77	GLN46 ARG49 GLN45 ASP332 GLY202	HIS145, MET146, ALA76, ASN78, GLY77, LYS192, ASP190, LYS97 GLN153	GLY91 GLN56 GLU144 MET146 ASP147 ARG201	TYR240, ASP208 GLY210, ARG234 ILE216, ASP190 LEU115, LYS97, ILE111, ILE139	MET146 GLY149 GLY75 SER150 GLN153 ASP190 ALA76
Unfavorable Donor-Donor		PHE333 (1.97)	SER194 (2.55)			

Keys: The values in bracket beside the interacting AA are the binding distance (Ă) between the ligand and the corresponding amino acid residues of the receptors.

NSC777213_PI3K, NSC777213_AKT, and NSC777213_mTOR complexes are stabilized by numerous π-interactions. The π-interactions mostly involve charge transfer between atoms, these interactions would undoubtedly have helped in intercalating NSC777213 in PI3K/AKT/mTOR binding cavities. Furthermore, Van der Waals forces created around the NSC-777213 backbone with the PRO789, TRP292, GLU880, CYS869, GLN846, and ILE870 residues of the PI3K, ALA214, ASN233, TYR231, GLU230, LYS285 and PHE439 of AKT; and, GLN1931, ILE1892, ASP1933, ASN2147, GLY1897 and LEU1936 of mTOR create a strong cohesive environment, which further stabilized the complexes [91]. Furthermore, we used Swiss dock, an online docking algorithm that estimates and scores the binding mode of receptor to ligand by using their FullFitness and clustered values [59], and we obtained similar results of binding affinities, namely -6.67, -7.18, and -7.68 for AKT, mTOR , and PI3K, respectively (Supplementary Table 5). Interactions of NSC777213 with the active site of human MEK-1 kinase (-7.9 kcal/mol) is based on the H-bond interactions with SER150, SER194 and MET145; π-Anion interaction with ASP152; and amide- π stacking with LEU74 which are supported by several Van der Waals forces (**Table 6**). Altogether, these molecular modeling experiments suggested that NSC777213 has the molecular properties to interact efficiently with the binding site of PI3K/AKT/mTOR/MEK.

In experimental scoring functions, binding energy are contributions of several energy modules, including ionic and hydrophobic interactions, hydrogen bonding, and binding entropies [88, 92]. Therefore, the unique high affinity and stability of NSC765690 in the binding site of PI3K could be collectively attributed to the high numbers of hydrogen bonds, halogen bonds, π-interactions, and Van der Waals forces. In addition, the high numbers of π interactions, including the π-π stacking with the aromatic rings of TRP201; π-cation with ARG690 and ARG849; and π alkylation with PHE698, LEU661, MET842, and HIS295, could enhance the selectivity and physiochemical features (lipophilicity, specificity, bioavailability, and metabolic stability) [93] of NSC765690 in PI3K binding site. Thus, NSC777213 has a higher targeting preference for PI3K than it does for AKT, mTOR and MEK.

When compared with the parental compound (isoflavone) NSC777213 displayed more robust interactions and higher affinities for AKT and mTOR. Our docking results revealed that the OCH3 and the 2-fluoro-4-iodoaniline motif attached to the isoflavone core of NSC777213 was quite important; we observed that these groups are responsible for forming additional 5 alkyl interactions, a pi-interaction, and 1 halogen interaction in the PI3K-NSC777213 complex when compared with the interaction in the isoflavone_PI3K complex (**Figure 8**). Furthermore, 2 conventional hydrogen bonds and a C-H bond interaction in the PI3K_NSC777213 complex are completely missing in the PI3K_isoflavone complex. However, the higher number of van der wall forces observed around the parental compound (isoflavone) in the pi3k active site could be responsible for its lower binding energy (-9.0 kcal/mol) to PI3K when compared with the binding energy of NSC777213 to PI3K (-8.0 kcal/mol) (**Table 5**). Furthermore, in addition to higher binding affinity (-7.0 kcal/mol) NSC777213 interacted with mTOR by 2 conventional H bonds (ASN1899 and GLN1937) and a C-H bond (THR1934) as opposed to only a single conventional H-bonding (GLN1937) in the mTOR_isoflavone complex (-6.8 kcal/mol) (**Figure 9**). Similarly, a higher number of interactions and stronger binding affinity (-6.7 kcal/mol) exist between AKT and NSC777213 than the interaction between AKT and isoflavone (**Figure 10**). The higher affinity and interaction of NSC777213 with AKT and mTOR would means higher inhibition of the cascade of phosphorylation events that lead to the activation of mTOR downstream component [1, 14] including 4EBP1 and S6K. Hence compromising the nutrient metabolism, protein synthesis, and translation initiation of cancer cells [15, 16].

Comparative MEK1 docking profile between NSC777213 and clinical MEK inhibitors revealed more robust interactions and higher binding affinity of NSC777213 (-7.9 kcal/mol) for human MEK-1 kinase (PDB: 3SLS) than does pimasertib (-7.60 kcal/mol), mirdametinib (-6.90 kcal/mol), and rafametinib (-7.4 kcal/mol), but has a comparable affinity with cobimetinib (-8.0 kcal/mol) (**Table 6**). However, owing to the higher conventional and non-conventional hydrogen bond interactions (**Figure 11**), TAK-733 demonstrates a higher affinity for

human MEK-1 kinase (-8.6 kcal/mol) than NSC777213. MEK promote cell proliferation, cell survival and metastasis via phosphorylation of ERK which regulate gene expression and various transcriptional factors [22]. The kinase domain of MEK-1 contains the ATP binding site and catalytic apparatus [94]. MEK inhibitors are either ATP non-competitive or ATP competitive inhibitors. The majority of MEK inhibitors in clinical development including the cobimetinib, pimasertib, refametinib, mirdametinib, and TAK-733 are ATP non-competitive i.e. they do not directly compete for the ATP-binding site, but rather bind to the allosteric site adjacent to ATP binding site [94]. This binding would inhibit the catalytic activity of MEK1, resulting in decreased phosphorylation and inactivation of ERK2 and hence decreased tumor cell proliferation. Considering the molecular docking analysis, NSC777213 is, therefore, likely to be a non-ATP-competitive MEK inhibitor. This likeliness would be of specificity advantage [95], however, further validation studies are required. Collectively, NSC777213 demonstrated robust interactions and higher affinities for AKT and mTOR than the isoflavone, and for MEK-1 than some MEK inhibitors under clinical developments, thus serve as a novel anti-cancer agent with potential for dual inhibition of PI3K/AKT/mTOR and MEK signaling pathways. Interestingly, our *in silico* mechanistic study was further validated by western blot analysis. We found that treatment of U251 and U87MG cells with NSC777213 significantly downregulated the expression levels of PI3K, AKT, mTOR, and MEK as well as the phosphorylated forms; p-AKT, p-mTOR, p-PI3K, and p-MEK (**Figure 11B**).

NSC777213 is a safe drug-likeness candidate for oral, intravenous, intraperitoneal, and subcutaneous administration

Computational approaches have led to the comprehensive understanding of ADMET properties though the interactive optimization of leads, mitigating the tendency of drug failure [96]. Our analysis of ADMET and physicochemical properties indicated that NSC777213 has desirable lipophilicity, polarity, flexibility, solubility, saturation, molecular weight, and other properties required for being a good drug candidate. It satisfies Lipinski, Ghose, Veber, and Egan's rules for drug likeness. Furthermore NSC777213 has a high probability of gastrointestinal absorption and bioavailability and can penetrate the blood-brain barrier unlike the MEK inhibitors under clinical developments (**Table 7**; Supplementary Figure 7). This BBB permeation ability of NSC777213 is an added advantage for treatments of glioblastoma. The BBB acts like a physiological barrier to protect the CNS from pathogens and toxins, but also impedes drug's efficacy in treatments of brain cancers [97]. Many of the MEK inhibitors in clinical development have limited ability to permeate the BBB, which in turn limit their therapeutic efficacy against glioblastoma [97, 98]. Employing the BBB-permeable NSC777213 for targeting GBM cells will enhance treatment outcome and decrease toxicities on normal cells [99]. In addition, the estimated LD_{50} in acute toxicity from oral, intravenous, intraperitoneal, and subcutaneous administration indicated that NSC777213 exhibited LD_{50} at a very high dose and thus was grouped as a member of the class 4 and 5 OECD classification of compounds. An ecotoxicological assessments using bioaccumulation factor (log10), *Daphnia magna* (LC_{50} log10), fathead minnow (LC_{50} log10), and *Tetrahymena pyriformis* (IGC_{50} log10), indicate a low toxity levels of 1.261 BCF, 6.998 mol/L, -2.671 mmol/L, and 1.552 mol/L, respectively, suggesting high envinronmental friendliness. Collectively, this finding suggested that NSC777213 meets the criteria for being a drug-likeness candidate and is safe for oral, intravenous, intraperitoneal, and subcutaneous administration.

Conclusions

In conclusion, our study showed that PI3K/AKT/mTOR/MEK is a crucial oncoimmune poor prognosticator signature in multiple cancers. We demonstrate that NSC777213, exhibit both antiproliferative activities against NCI60 human tumor cell lines and a selective cytotoxic preference for NSCLC, melanoma, CNS, renal, and ovarian cancer cell lines. In addition, NSC777213 demonstrate robust binding interactions and higher affinities for AKT and mTOR than did isoflavone, and also demonstrate a higher affinity for human MEK-1 kinase than some MEK inhibitors under clinical developments. Our study suggests that NSC777213 is a promising PI3K/AKT/mTOR/MEK inhibitor for further preclinical and clinical evaluation as a

Table 7. Drug likeness, medicinal chemistry and physicochemical and toxicity properties of NSC777213

Properties	NSC777213	Cobimetinib	Pimasertib	Refametinib	Mirdametinib	TAK-733	Reference Value
Formula	C15H9FIN04	C21H21F3IN302	C15H15FIN303	C19H20F3IN2O5S	C16H14F3IN2O4	C17H15F2IN404	-
M.W (g/mol)	413.14	531.3	431.2	572.3	482.189	504.23	150-500
R-bonds	2	5	7	9	8	5	0-9
H-bond ACC.	5	6	5	8	7	7	0-10
H-bond DON.	0	3	4	4	4	3	0-5
Molar Refractivity	87.25	122.92	91.39	117.62	94.60	106.90	
TPSA ($Å^2$)	61.44	64.60	94.48	116.27	90.82	109.38	20-130
Fraction Csp3	0.07	0.38	0.20	0.37	0.19	0.24	0.25~< 1
Log Po/w (XLOGP3)	3.48	3.88	1.67	2.90	2.99	0.85	-0.7~5
Consensus Log Po/w	3.42	4.10	1.91	3.56	3.05	1.98	
Log S (ESOL)	-5.00	-5.54	-3.49	-4.83	-4.53	-3.59	0-6
Drug-likeness (Lipinski rule)	Yes; 0 violation	Yes; 1 violation	Yes; 0 violation	Yes; 1 violation	Yes; 0 violation	Yes; 1 violation	
Bioavailability Score	0.55	0.55	0.55	0.55	0.55	0.55	> 0.1 (10%)
BBB-permeation	YES	YES	NO	No	No	No	
Synthetic accessibility	3.24	3.92	3.40	4.48	3.83	3.75	1 (very easy) to 10 (very difficult).
Route of adm.	Acute toxicity in rats (LD_{50} (mg/kg))						
Intraperitoneal	526.400 (OECD:5)	213.700	577.800	2624.00	1540.000	818.400	
Intravenous	336.600 (OECD:5)	75.620	2203.300	251.300	831.000	808.900	
Oral	724.400 (OECD:4)	449.900	782.200	2252.000	1909.000	1494.000	
Subcutaneous	890.400 (OECD:4)	363.300	806.500	507.800	645.200	251.900	
	Ecotoxicity						
Bioaccumulation factor Log10 (BCF)	1.261	0.860	0.289	0.422	0.885	0.226	
Daphnia magna LC_{50} -Log10 (mol/L)	6.998	7.335	5.820	6.122	6.458	5.947	
Fathead Minnow LC_{50} Log10 (mmol/L)	-2.671	-4.230	-2.177	-3.512	-3251	-2.671	
Tetrahymena pyriformis IGC_{50} -Log10 (mol/L)	1.552	2.056	1.160	1.477	1.556	1.112	

R-bond; Num. rotatable bonds; H-bond ACC; Num. H-bond acceptors, H-bond DON; H-bond donors, BBB; Blood brain barrier, IP; Intraperitoneal, IV; Intravenous, SC; Subcutaneous.

chemotherapeutic agent, particularly for the treatment of NSCLC, melanoma, and brain, renal, and ovarian cancers.

Acknowledgements

We acknowledge the NCI Developmental Therapeutics Program (DTP) for the NCI60-cancer-cell-line screening of NSC777213, funded by the National Cancer Institute, National Institutes of Health (NIH-NCI). Hsu-Shan Huang is funded by the Ministry of Science and Technology, Taiwan (MOST 109-2113-M-038-003).

Disclosure of conflict of interest

None.

Address correspondence to: Alexander TH Wu, TMU Research Center of Cancer Translational Medicine, Taipei Medical University, Taipei 11031, Taiwan. E-mail: chaw1211@tmu.edu.tw; Hsu-Shan Huang, PhD Program for Cancer Molecular Biology and Drug Discovery, College of Medical Science and Technology, Taipei Medical University and Academia Sinica, Taipei 11031, Taiwan. E-mail: huanghs99@tmu.edu.tw

References

[1] Samuels Y and Ericson K. Oncogenic PI3K and its role in cancer. Curr Opin Oncol 2006; 18: 77-82.

[2] Fruman DA and Rommel C. PI3K and cancer: lessons, challenges and opportunities. Nat Rev Drug Discov 2014; 13: 140-156.

[3] Carneiro BA, Kaplan JB, Altman JK, Giles FJ and Platanias LC. Targeting mTOR signaling pathways and related negative feedback loops for the treatment of acute myeloid leukemia. Cancer Chemother Pharmacol 2015; 16: 648-656.

[4] Darici S, Alkhaldi H, Horne G, Jørgensen HG, Marmiroli S and Huang X. Targeting PI3K/Akt/mTOR in AML: rationale and clinical evidence. J Clin Med 2020; 9: 2934.

[5] Thorpe LM, Yuzugullu H and Zhao JJ. PI3K in cancer: divergent roles of isoforms, modes of activation and therapeutic targeting. Nat Rev Cancer 2015; 15: 7-24.

[6] Porta C, Paglino C and Mosca A. Targeting PI3K/Akt/mTOR signaling in cancer. Front Oncol 2014; 4: 64-64.

[7] Zhao JJ and Roberts TM. PI3 kinases in cancer: from oncogene artifact to leading cancer target. Sci STKE 2006; 2006: pe52-pe52.

[8] Asati V, Mahapatra DK and Bharti SK. PI3K/Akt/mTOR and Ras/Raf/MEK/ERK signaling pathways inhibitors as anticancer agents: Structural and pharmacological perspectives. Eur J Med Chem 2016; 109: 314-341.

[9] Manning BD and Toker A. AKT/PKB signaling: navigating the network. Cell 2017; 169: 381-405.

[10] Saxton RA and Sabatini DM. mTOR signaling in growth, metabolism, and disease. Cell 2017; 168: 960-976.

[11] Weinberg MA. RES-529: a PI3K/AKT/mTOR pathway inhibitor that dissociates the mTORC1 and mTORC2 complexes. Anticancer Drugs 2016; 27: 475-487.

[12] Meng D, Frank AR and Jewell JL. mTOR signaling in stem and progenitor cells. Development 2018; 145: dev152595.

[13] Guimarães IS, Tessarollo NG, Lyra-Junior P, dos Santos DZ, Zampier RC, de Oliveira L, Siqueira KV, Silva IV and Rangel L. Targeting the PI3K/AKT/mTOR pathway in cancer cells. Updates on Cancer Treatment 2015.

[14] Kim LC, Cook RS and Chen J. mTORC1 and mTORC2 in cancer and the tumor microenvironment. Oncogene 2017; 36: 2191-2201.

[15] Fruman DA, Chiu H, Hopkins BD, Bagrodia S, Cantley LC and Abraham RT. The PI3K pathway in human disease. Cell 2017; 170: 605-635.

[16] Dibble CC and Cantley LC. Regulation of mTORC1 by PI3K signaling. Trends Cell Biol 2015; 25: 545-555.

[17] Ebner M, Sinkovics B, Szczygieł M, Ribeiro DW and Yudushkin I. Localization of mTORC2 activity inside cells. J Cell Biol 2017; 216: 343-353.

[18] Jhanwar-Uniyal M, Wainwright JV, Mohan AL, Tobias ME, Murali R, Gandhi CD and Schmidt MH. Diverse signaling mechanisms of mTOR complexes: mTORC1 and mTORC2 in forming a formidable relationship. Adv Biol Regul 2019; 72: 51-62.

[19] Rad E, Murray JT and Tee AR. Oncogenic signalling through mechanistic target of rapamycin (mTOR): a driver of metabolic transformation and cancer progression. Cancers 2018; 10: 5.

[20] Chen QY and Costa M. PI3K/Akt/mTOR signaling pathway and the biphasic effect of arsenic in carcinogenesis. Mol Pharmacol 2018; 94: 784-792.

[21] Forbes SA, Bindal N, Bamford S, Cole C, Kok CY, Beare D, Jia M, Shepherd R, Leung K and Menzies A. COSMIC: mining complete cancer genomes in the Catalogue of Somatic Mutations in Cancer. Nucleic Acids Res 2010; 39: D945-D950.

[22] Roberts PJ and Der CJ. Targeting the Raf-MEK-ERK mitogen-activated protein kinase cascade

for the treatment of cancer. Oncogene 2007; 26: 3291-3310.
[23] Butt G, Shahwar D, Qureshi MZ, Attar R, Akram M, Birinci Y, Karatoprak GS, Gasparri ML and Farooqi AA. Role of mTORC1 and mTORC2 in breast cancer: therapeutic targeting of mTOR and its partners to overcome metastasis and drug resistance. Adv Exp Med Biol 2019; 1152: 283-292.
[24] Zou Z, Chen J, Yang J and Bai X. Targeted inhibition of Rictor/mTORC2 in cancer treatment: a new era after rapamycin. Curr Cancer Drug Targets 2016; 16: 288-304.
[25] De Santis MC, Gulluni F, Campa CC, Martini M and Hirsch E. Targeting PI3K signaling in cancer: challenges and advances. Biochim Biophys Acta Rev Cancer 2019; 1871: 361-366.
[26] Esposito A, Viale G and Curigliano G. Safety, tolerability, and management of toxic effects of phosphatidylinositol 3-kinase inhibitor treatment in patients with cancer: a review. JAMA Oncol 2019; 5: 1347-1354.
[27] Alzahrani AS. PI3K/Akt/mTOR inhibitors in cancer: at the bench and bedside. Semin Cancer Biol 2019; 59: 125-132.
[28] Cragg GM, Grothaus PG and Newman DJ. Impact of natural products on developing new anti-cancer agents. Chem Rev 2009; 109: 3012-3043.
[29] Cragg GM and Newman DJ. Natural products: a continuing source of novel drug leads. Biochim Biophys Acta 2013; 1830: 3670-3695.
[30] Lawal B, Shittu OK, Oibiokpa FI, Berinyuy EB and Mohammed H. African natural products with potential antioxidants and hepatoprotectives properties: a review. Clinical Phytoscience 2016; 2: 23.
[31] Lawal B, Shittu OK, Oibiokpa FI, Mohammed H, Umar SI and Haruna GM. Antimicrobial evaluation, acute and sub-acute toxicity studies of Allium sativum. Journal of Acute Disease 2016; 5: 296-301.
[32] Yusuf AA, Lawal B, Yusuf MA, Adejoke AO, Raji FH and Wenawo DL. Free radical scavenging, antimicrobial activities and effect of sub-acute exposure to Nigerian Xylopia Aethiopica seed extract on liver and kidney functional indices of albino rat. Iranian Journal of Toxicology 2018; 12: 51-58.
[33] Liu M, Qi Z, Liu B, Ren Y, Li H, Yang G and Zhang Q. RY-2f, an isoflavone analog, overcomes cisplatin resistance to inhibit ovarian tumorigenesis via targeting the PI3K/AKT/mTOR signaling pathway. Oncotarget 2015; 6: 25281-25294.
[34] Aamir A, Bernhard B, Yiwei L, Dejuan K, Bin B, Rainer S, Subhash BP and Fazlul HS. Deregulation of PI3K/Akt/mTOR signaling pathways by isoflavones and its implication in cancer treatment. Anticancer Agents Med Chem 2013; 13: 1014-1024.
[35] Chandrashekar DS, Bashel B, Balasubramanya SAH, Creighton CJ, Ponce-Rodriguez I, Chakravarthi B and Varambally S. UALCAN: a portal for facilitating tumor subgroup gene expression and survival analyses. Neoplasia 2017; 19: 649-658.
[36] Tang Z, Li C, Kang B, Gao G, Li C and Zhang Z. GEPIA: a web server for cancer and normal gene expression profiling and interactive analyses. Nucleic Acids Res 2017; 45: W98-W102.
[37] Li T, Fu J, Zeng Z, Cohen D, Li J, Chen Q, Li B and Liu XS. TIMER2.0 for analysis of tumor-infiltrating immune cells. Nucleic Acids Res 2020; 48: W509-W514.
[38] Poroikov VV, Filimonov DA, Gloriozova TA, Lagunin AA, Druzhilovskiy DS, Rudik AV, Stolbov LA, Dmitriev AV, Tarasova OA, Ivanov SM and Pogodin PV. Computer-aided prediction of biological activity spectra for organic compounds: the possibilities and limitations. Russian Chemical Bulletin 2019; 68: 2143-2154.
[39] Daina A, Michielin O and Zoete V. SwissADME: a free web tool to evaluate pharmacokinetics, drug-likeness and medicinal chemistry friendliness of small molecules. Sci Rep 2017; 7: 42717.
[40] Lipinski CA. Lead-and drug-like compounds: the rule-of-five revolution. Drug Discov Today Technol 2004; 1: 337-341.
[41] Martin YC. A bioavailability score. J Med Chem 2005; 48: 3164-3170.
[42] Daina A and Zoete V. A BOILED-egg to predict gastrointestinal absorption and brain penetration of small molecules. ChemMedChem 2016; 11: 1117-1121.
[43] Lagunin AA, Zakharov AV, Filimonov DA and Poroikov VV. A new approach to QSAR modelling of acute toxicity. SAR QSAR Environ Res 2007; 18: 285-298.
[44] Shoemaker RH. The NCI60 human tumour cell line anticancer drug screen. Nat Rev Cancer2006; 6: 813-823.
[45] Holbeck SL, Collins JM and Doroshow JH. Analysis of Food and Drug Administration-approved anticancer agents in the NCI60 panel of human tumor cell lines. Mol Cancer Ther 2010; 9: 1451-1460.
[46] Vichai V and Kirtikara K. Sulforhodamine B colorimetric assay for cytotoxicity screening. Nat Protoc 2006; 1: 1112-1116.
[47] Lisanti MP, Martinez-Outschoorn UE and Sotgia F. Oncogenes induce the cancer-associated fibroblast phenotype: metabolic symbiosis and "fibroblast addiction" are new therapeutic targets for drug discovery. Cell Cycle 2013; 12: 2723-2732.

[48] Boyd MR and Paull KD. Some practical considerations and applications of the National Cancer Institute in vitro anticancer drug discovery screen. Drug Dev Res 1995; 34: 91-109.
[49] Paull K, Shoemaker R, Hodes L, Monks A, Scudiero D, Rubinstein L, Plowman J and Boyd M. Display and analysis of patterns of differential activity of drugs against human tumor cell lines: development of mean graph and COMPARE algorithm. J Natl Cancer Inst 1989; 81: 1088-1092.
[50] Lawal B, Liu YL, Mokgautsi N, Khedkar H, Sumitra MR, Wu ATH and Huang HS. Pharmacoinformatics and preclinical studies of NSC-765690 and NSC765599, potential STAT3/CDK2/4/6 Inhibitors with antitumor activities against NCI60 human tumor cell lines. Biomedicines 2021; 9: 92.
[51] Gfeller D, Michielin O and Zoete V. Shaping the interaction landscape of bioactive molecules. Bioinformatics 2013; 29: 3073-3079.
[52] Liu X, Ouyang S, Yu B, Liu Y, Huang K, Gong J, Zheng S, Li Z, Li H and Jiang H. PharmMapper server: a web server for potential drug target identification using pharmacophore mapping approach. Nucleic Acids Res 2010; 38: W609-W614.
[53] Mahmood T and Yang PC. Western blot: technique, theory, and trouble shooting. N Am J Med Sci 2012; 4: 429-434.
[54] Hanwell MD, Curtis DE, Lonie DC, Vandermeersch T, Zurek E and Hutchison GR. Avogadro: an advanced semantic chemical editor, visualization, and analysis platform. J Cheminform 2012; 4: 17.
[55] Trott O and Olson AJ. AutoDock Vina: improving the speed and accuracy of docking with a new scoring function, efficient optimization, and multithreading. J Comput Chem 2010; 31: 455-461.
[56] Lee JC, Wu ATH, Chen JH, Huang WY, Lawal B, Mokgautsi N, Huang HS and Ho CL. HNC0014, a multi-targeted small-molecule, inhibits head and neck squamous cell carcinoma by suppressing c-Met/STAT3/CD44/PD-L1 oncoimmune signature and eliciting antitumor immune responses. Cancers 2020; 12: 3759.
[57] Lawal B, Lee CY, Mokgautsi N, Sumitra MR, Khedkar H, Wu ATH and Huang HS. mTOR/EGFR/iNOS/MAP2K1/FGFR/TGFB1 Are Druggable Candidates for N-(2,4-Difluorophenyl)-2',4'-Difluoro-4-Hydroxybiphenyl-3-Carboxamide (NSC765598), With Consequent Anticancer Implications. Front Oncol 2021; 11: 656738.
[58] Visualizer DS. BIOVIA, Dassault Systèmes, BIOVIA Workbook, Release 2020; BIOVIA Pipeline Pilot, Release 2020. San Diego: Dassault Systèmes; 2020.
[59] Grosdidier A, Zoete V and Michielin O. EADock: docking of small molecules into protein active sites with a multiobjective evolutionary optimization. Proteins 2007; 67: 1010-1025.
[60] Nie Y, Liu L, Liu Q and Zhu X. Identification of a metabolic-related gene signature predicting the overall survival for patients with stomach adenocarcinoma. PeerJ 2021; 9: e10908.
[61] Faubert B, Solmonson A and DeBerardinis RJ. Metabolic reprogramming and cancer progression. Science 2020; 368: eaaw5473.
[62] Murugan AK. mTOR: role in cancer, metastasis and drug resistance. Semin Cancer Biol 2019; 59: 92-111.
[63] McCubrey JA, Abrams SL, Fitzgerald TL, Cocco L, Martelli AM, Montalto G, Cervello M, Scalisi A, Candido S, Libra M and Steelman LS. Roles of signaling pathways in drug resistance, cancer initiating cells and cancer progression and metastasis. Adv Biol Regul 2015; 57: 75-101.
[64] Muz B, de la Puente P, Azab F and Azab AK. The role of hypoxia in cancer progression, angiogenesis, metastasis, and resistance to therapy. Hypoxia (Auckl) 2015; 3: 83-92.
[65] Li B, Jiang Y, Li G, Fisher GA Jr and Li R. Natural killer cell and stroma abundance are independently prognostic and predict gastric cancer chemotherapy benefit. JCI Insight 2020; 5: e136570.
[66] Ino Y, Yamazaki-Itoh R, Shimada K, Iwasaki M, Kosuge T, Kanai Y and Hiraoka N. Immune cell infiltration as an indicator of the immune microenvironment of pancreatic cancer. Br J Cancer 2013; 108: 914-923.
[67] Wu M, Li X, Zhang T, Liu Z and Zhao Y. Identification of a nine-gene signature and establishment of a prognostic nomogram predicting overall survival of pancreatic cancer. Front Oncol 2019; 9: 996-996.
[68] Hiraoka N, Onozato K, Kosuge T and Hirohashi S. Prevalence of FOXP3+ regulatory T cells increases during the progression of pancreatic ductal adenocarcinoma and its premalignant lesions. Clin Cancer Res 2006; 12: 5423-5434.
[69] Zhang Y, Yan W, Mathew E, Bednar F, Wan S, Collins MA, Evans RA, Welling TH, Vonderheide RH and di Magliano MP. CD4+ T lymphocyte ablation prevents pancreatic carcinogenesis in mice. Cancer Immunol Res2014; 2: 423-435.
[70] Borst J, Ahrends T, Bąbała N, Melief CJ and Kastenmüller W. CD4+ T cell help in cancer immunology and immunotherapy. Nat Rev Immunol 2018; 18: 635-647.
[71] Kennedy R and Celis E. Multiple roles for CD4+ T cells in anti-tumor immune responses. Immunol Rev 2008; 222: 129-144.
[72] Tarantino G and Capone D. Inhibition of the mTOR pathway: a possible protective role in

coronary artery disease. Ann Med 2013; 45: 348-356.
[73] Wang L, Wei Q, Zhang M, Chen L, Li Z, Zhou C, He M, Wei M and Zhao L. Identification of the prognostic value of immune gene signature and infiltrating immune cells for esophageal cancer patients. Int Immunopharmacol 2020; 87: 106795.
[74] Burney IA and Al-Moundhri MS. Major advances in the treatment of cancer: what does a non-oncologist need to know? Sultan Qaboos Univ Med J 2008; 8: 137-148.
[75] Lu B, Huang S, Cao J, Hu Q, Shen R, Wan H, Wang D, Yuan J, Zhang L, Zhang J, Zhang M, Tao W and Zhang L. Discovery of EBI-1051: a novel and orally efficacious MEK inhibitor with benzofuran scaffold. Bioorg Med Chem 2018; 26: 581-589.
[76] Chen CL, Liu FL, Lee CC, Chen TC, Ahmed Ali AA, Sytwu HK, Chang DM and Huang HS. Modified salicylanilide and 3-Phenyl-2H-benzo[e][1,3]oxazine-2,4(3H)-dione derivatives as novel inhibitors of osteoclast differentiation and bone resorption. J Med Chem 2014; 57: 8072-8085.
[77] Luzina EL and Popov AV. Synthesis and anticancer activity evaluation of 3,4-mono- and bicyclosubstituted N-(het)aryl trifluoromethyl succinimides. J Fluor Chem 2014; 168: 121-127.
[78] Coussens NP, Braisted JC, Peryea T, Sittampalam GS, Simeonov A and Hall MD. Small-molecule screens: a gateway to cancer therapeutic agents with case studies of food and drug administration-approved drugs. Pharmacol Rev 2017; 69: 479-496.
[79] Hamilton TC, Young RC, McKoy WM, Grotzinger KR, Green JA, Chu EW, Whang-Peng J, Rogan AM, Green WR and Ozols RF. Characterization of a human ovarian carcinoma cell line (NIH:OVCAR-3) with androgen and estrogen receptors. Cancer Res 1983; 43: 5379-5389.
[80] Louie KG, Behrens BC, Kinsella TJ, Hamilton TC, Grotzinger KR, McKoy WM, Winker MA and Ozols RF. Radiation survival parameters of antineoplastic drug-sensitive and -resistant human ovarian cancer cell lines and their modification by buthionine sulfoximine. Cancer Res 1985; 45: 2110-2115.
[81] Lorenzi PL, Reinhold WC, Varma S, Hutchinson AA, Pommier Y, Chanock SJ and Weinstein JN. DNA fingerprinting of the NCI-60 cell line panel. Mol Cancer Ther 2009; 8: 713-724.
[82] Bates SE, Fojo AT, Weinstein JN, Myers TG, Alvarez M, Pauli KD and Chabner BA. Molecular targets in the National Cancer Institute drug screen. J Cancer Res Clin Oncol 1995; 121: 495-500.
[83] Subtel'na I, Atamanyuk D, Szymańska E, Kieć-Kononowicz K, Zimenkovsky B, Vasylenko O, Gzella A and Lesyk R. Synthesis of 5-arylidene-2-amino-4-azolones and evaluation of their anticancer activity. Bioorg Med Chem 2010; 18: 5090-102.
[84] Agamah FE, Mazandu GK, Hassan R, Bope CD, Thomford NE, Ghansah A and Chimusa ER. Computational/in silico methods in drug target and lead prediction. Brief Bioinform 2019; 21: 1663-1675.
[85] Zheng M, Chen L and Hua L. Chapter 17 - in silico modeling of FDA-approved drugs for discovery of anticancer agents: a drug-repurposing approach. In: Roy K, editor. In Silico Drug Design: Academic Press; 2019. pp. 527-548.
[86] Daina A, Michielin O and Zoete V. SwissTargetPrediction: updated data and new features for efficient prediction of protein targets of small molecules. Nucleic Acids Res 2019; 47: W357-W364.
[87] Kitchen DB, Decornez H, Furr JR and Bajorath J. Docking and scoring in virtual screening for drug discovery: methods and applications. Nat Rev Drug Discov 2004; 3: 935-949.
[88] Meng XY, Zhang HX, Mezei M and Cui M. Molecular docking: a powerful approach for structure-based drug discovery. Curr Neuropharmacol 2011; 7: 146-157.
[89] Jorgensen WL. The many roles of computation in drug discovery. Science 2004; 303: 1813-1818.
[90] Zhao H and Huang D. Hydrogen bonding penalty upon ligand binding. PLoS One 2011; 6: e19923.
[91] Arthur DE and Uzairu A. Molecular docking studies on the interaction of NCI anticancer analogues with human Phosphatidylinositol 4,5-bisphosphate 3-kinase catalytic subunit. Journal of King Saud University - Science 2019; 31: 1151-1166.
[92] Böhm HJ. Prediction of binding constants of protein ligands: a fast method for the prioritization of hits obtained from de novo design or 3D database search programs. J Comput Aided Mol Des 1998; 12: 309-309.
[93] Liang Z and Li QX. π-cation interactions in molecular recognition: perspectives on pharmaceuticals and pesticides. J Agric Food Chem 2018; 66: 3315-3323.
[94] Akinleye A, Furqan M, Mukhi N, Ravella P and Liu D. MEK and the inhibitors: from bench to bedside. Haematologica 2013; 6: 1-11.
[95] Eli MW, Joseph PL, Tammie Y, James DW and Kevin K. Progress towards therapeutic small molecule mek inhibitors for use in cancer therapy. Curr Top Med Chem 2005; 5: 215-229.
[96] Zhang W, Pei J and Lai L. Computational multitarget drug design. J Chem Inf Model 2017; 57: 403-412.
[97] Gampa G, Kim M, Cook-Rostie N, Laramy JK, Sarkaria JN, Paradiso L, DePalatis L and El-

mquist WF. Brain distribution of a novel MEK inhibitor E6201: implications in the treatment of melanoma brain metastases. Drug Metab Dispos 2018; 46: 658-666.

[98] Agarwal S, Sane R, Oberoi R, Ohlfest JR and Elmquist WF. Delivery of molecularly targeted therapy to malignant glioma, a disease of the whole brain. Expert Rev Mol Med 2011; 13: e17-e17.

[99] Zhao HF, Wang J, Shao W, Wu CP, Chen ZP, To ST and Li WP. Recent advances in the use of PI3K inhibitors for glioblastoma multiforme: current preclinical and clinical development. Mol Cancer 2017; 16: 100.

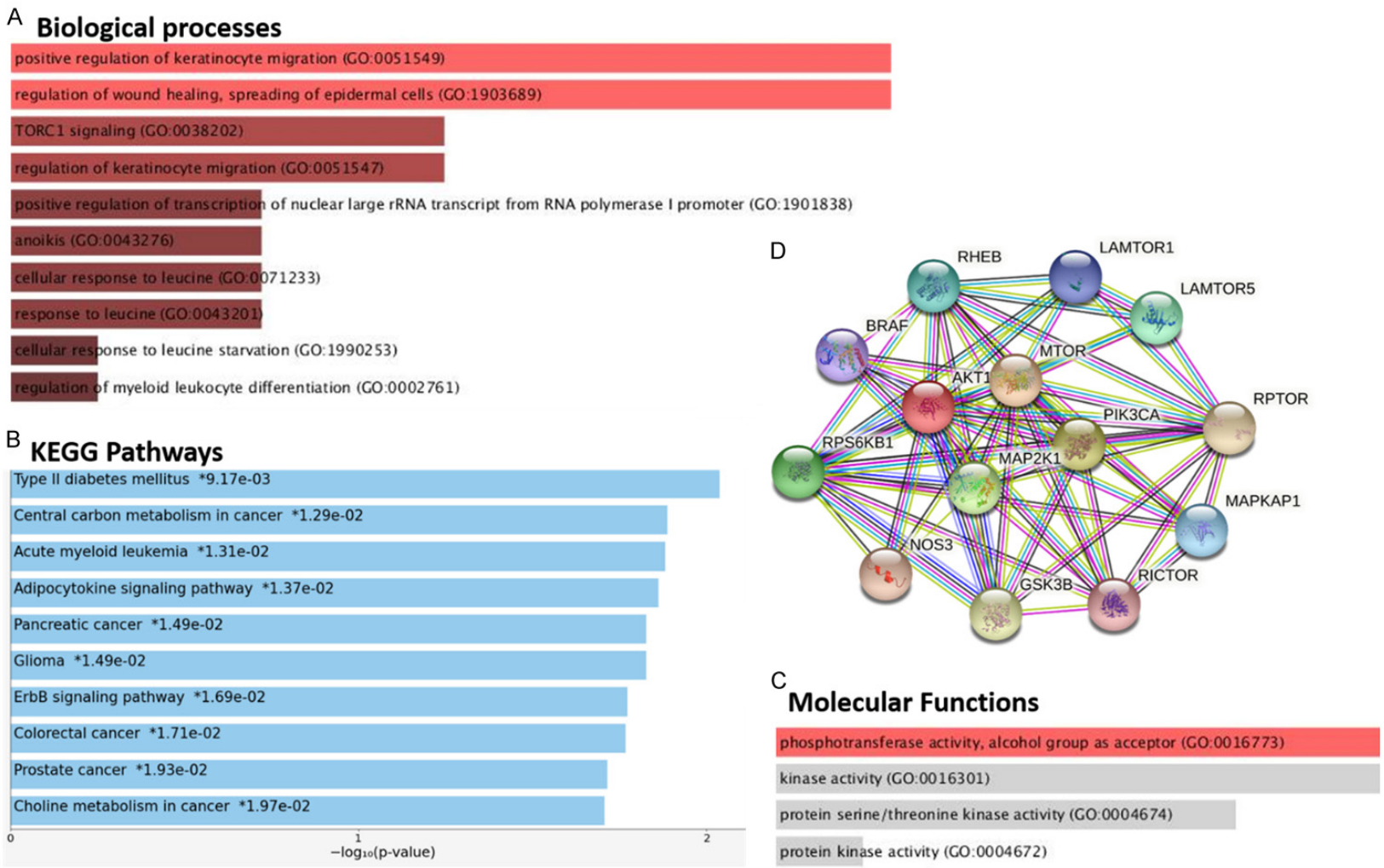

Supplementary Figure 1. Functional Enrichment and PPI Network of PI3K/AKT/mTOR/MEK Signature. The (A) biological process (B) Enriched Kyoto Encyclopedia of Genes and Genomes (KEGG) pathway and (C) molecular functions of PI3K/AKT/mTOR/MEK signature. (D) Protein-protein interaction (PPI) network of PI3K/AKT/mTOR/MEK signature. Second-order clustering of PI3K/AKT/mTOR/MEK signature generated 14 nodes, 62 edges, 8.86 average node degrees, an 0.852 average local clustering coefficient, and a PPI enrichment *p-value* of 4.44e-16.

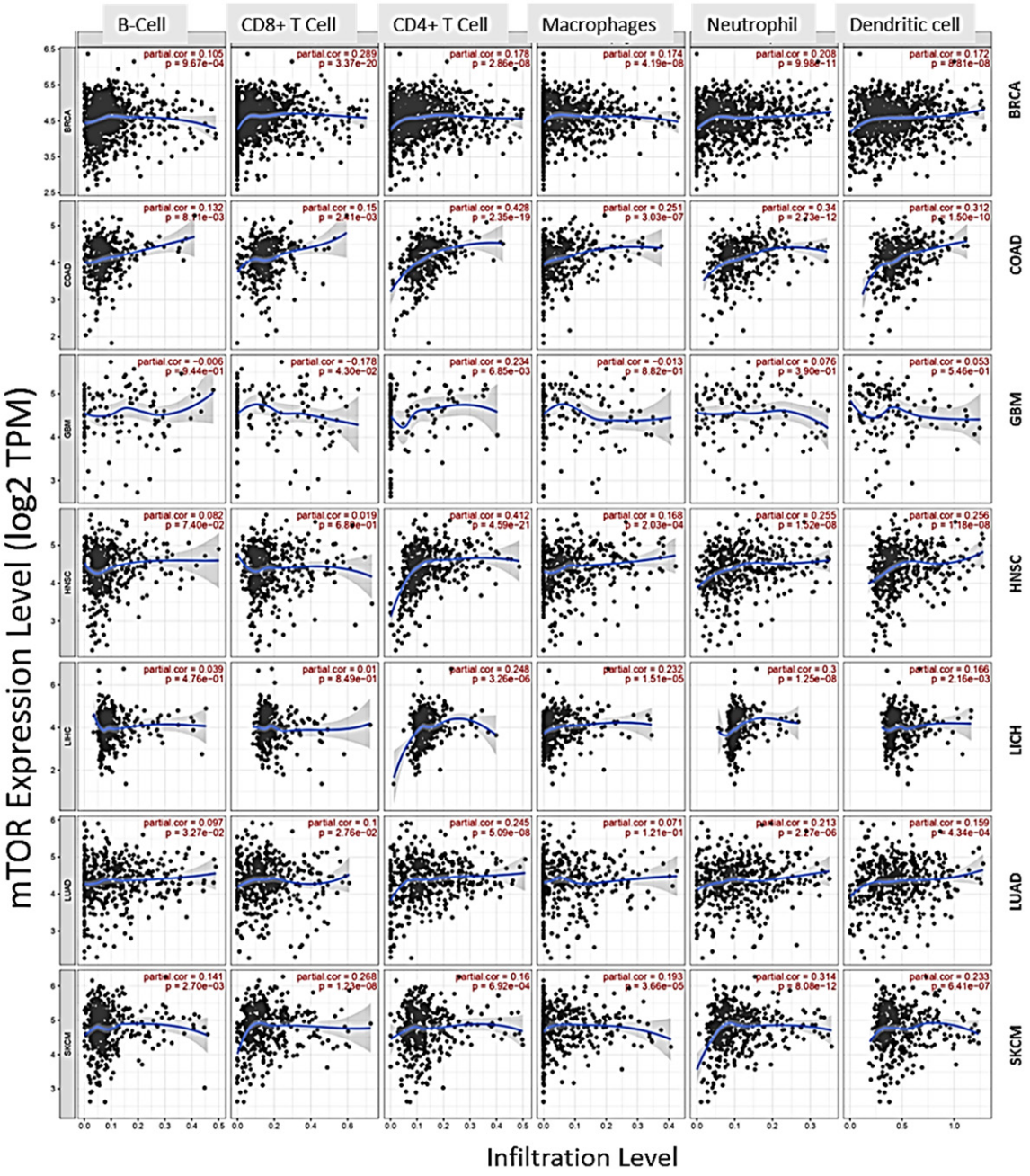

Supplementary Figure 2. Scatterplots of mTOR expression correlations with infiltrations of various immune cells in multiple cancer types. The strength of correlations is reflected by the purity-adjusted partial spearman's rho value, where a value of $r = 1$ means a perfect positive correlation and a value of $r = -1$ means a perfect negative correlation. SKCE, Skin cutaneous melanoma; LUAD, Lung adenocarcinoma; LIHC, Liver hepatocellular carcinoma; HNSC, Head and neck cancer; GBM, glioblastoma; BRCA, Breast invasive carcinoma; COAD, colon adenocarcinoma.

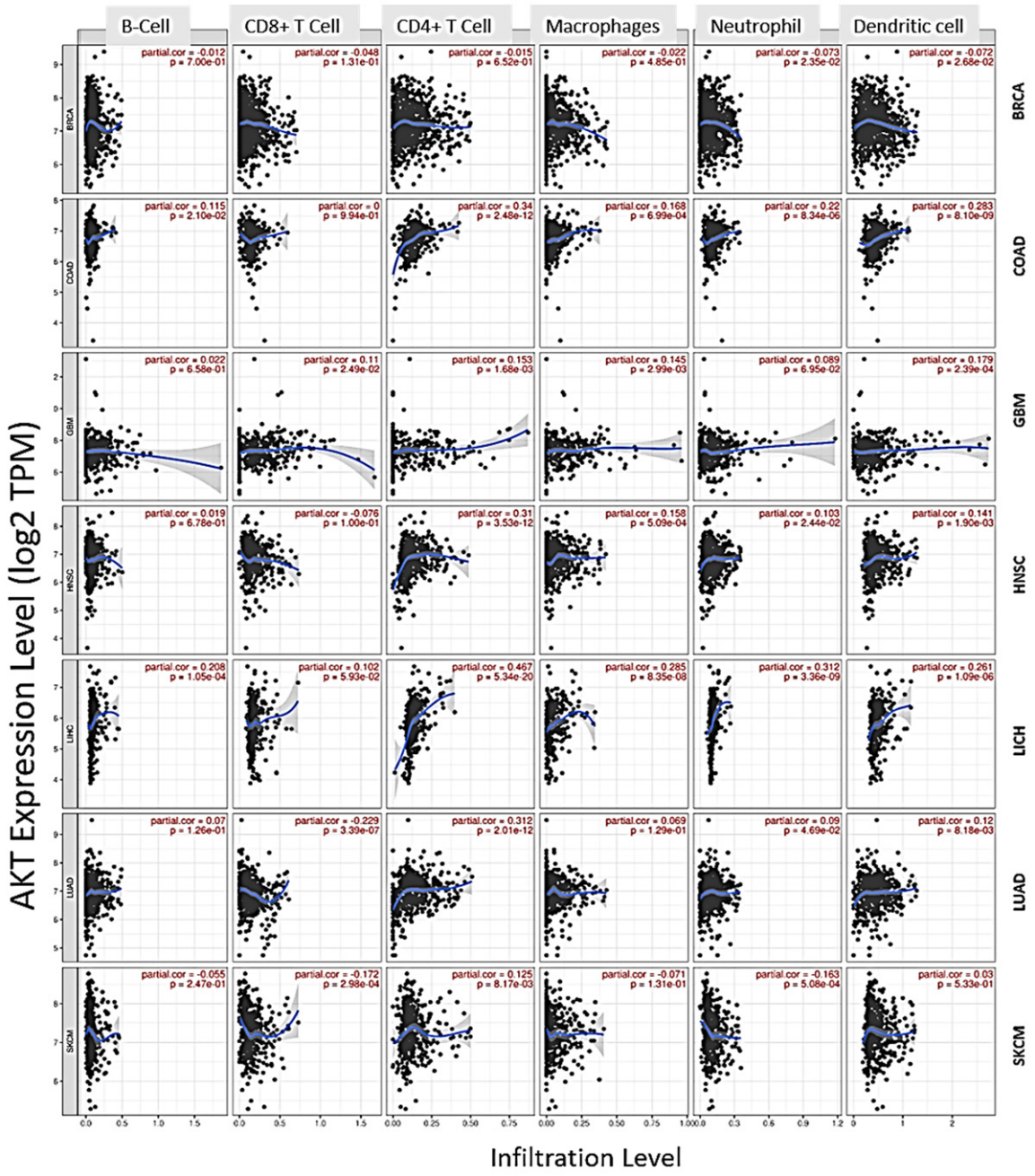

Supplementary Figure 3. Scatterplots of AKT expression correlations with infiltrations of various immune cells in multiple cancer types. The strength of correlations is reflected by the purity-adjusted partial spearman's rho value, where a value of $r = 1$ means a perfect positive correlation and a value of $r = -1$ means a perfect negative correlation. SKCE, Skin cutaneous melanoma; LUAD, Lung adenocarcinoma; LIHC, Liver hepatocellular carcinoma; HNSC, Head and neck cancer; GBM, glioblastoma; BRCA, Breast invasive carcinoma; COAD, colon adenocarcinoma.

Supplementary Table 1. Correlations of PI3K/AKT/mTOR/MET expressions with infiltrations of various immune cells in multiple cancer types

Cancers		MTOR		MET		PIK3CA		AKT	
cancer	Variables	partial.cor	*p*-value	partial.cor	*p*-value	partial.cor	*p*-value	partial.cor	*p*-value
BRCA	Purity	0.01451	0.647566	-0.38359	3.14E-36	-0.03316	0.295982	0.033953	0.284635
BRCA	B Cell	0.105414	0.000967	0.095693	0.002752	0.139163	1.27E-05	-0.01235	0.699743
BRCA	$CD8^+$ T Cell	0.288763	3.37E-20	0.343394	2.14E-28	0.453989	8.58E-51	-0.04839	0.130854
BRCA	$CD4^+$ T Cell	0.17773	2.86E-08	0.232759	2.66E-13	0.220555	4.61E-12	-0.01457	0.651795
BRCA	Macrophage	0.173763	4.19E-08	0.116201	0.000261	0.3302	1.95E-26	-0.0223	0.485005
BRCA	Neutrophil	0.207698	9.98E-11	0.228596	9.68E-13	0.375708	3.00E-33	-0.07345	0.023496
BRCA	Dendritic Cell	0.172401	8.81E-08	0.238887	8.30E-14	0.278842	1.92E-18	-0.07182	0.026782
COAD	Purity	-0.10722	0.030562	0.01029	0.836045	-0.13166	0.007824	-0.1467	0.003011
COAD	B Cell	0.131545	0.008113	0.134019	0.006985	0.266794	5.18E-08	0.114795	0.021008
COAD	$CD8^+$ T Cell	0.150208	0.002409	0.152658	0.002038	0.383332	1.17E-15	0.000346	0.994455
COAD	$CD4^+$ T Cell	0.428204	2.35E-19	0.259385	1.33E-07	0.568399	8.95E-36	0.339959	2.48E-12
COAD	Macrophage	0.251474	3.03E-07	0.212569	1.64E-05	0.562985	3.73E-35	0.167975	0.000699
COAD	Neutrophil	0.339728	2.73E-12	0.185771	0.000183	0.470947	1.58E-23	0.220485	8.34E-06
COAD	Dendritic Cell	0.312433	1.50E-10	0.201488	4.72E-05	0.499712	8.80E-27	0.282601	8.10E-09
GBM	Purity	0.370373	7.77E-06	-0.39004	1.13E-16	0.082976	0.089822	0.083791	0.086703
GBM	B Cell	-0.00627	0.944472	-0.21885	6.30E-06	-0.01543	0.753072	0.021685	0.658428
GBM	$CD8^+$ T Cell	-0.1778	0.042992	-0.16302	0.000822	-0.03359	0.493478	0.109693	0.024914
GBM	$CD4^+$ T Cell	0.234296	0.006851	0.010069	0.837374	0.060662	0.215845	0.153185	0.001683
GBM	Macrophage	-0.01315	0.881514	-0.07199	0.141757	0.134476	0.005894	0.144851	0.002995
GBM	Neutrophil	0.076006	0.390077	-0.03418	0.485811	0.123038	0.011817	0.088888	0.069453
GBM	Dendritic Cell	0.053076	0.54556	0.357631	4.67E-14	0.200395	3.68E-05	0.178762	0.000239
HNSC	Purity	-0.01257	0.780725	-0.01093	0.80876	0.098997	0.027956	0.113449	0.011712
HNSC	B Cell	0.081967	0.074	-0.15036	0.001	0.133268	0.003581	0.019103	0.677615
HNSC	$CD8^+$ T Cell	0.018984	0.68015	-0.16081	0.00044	0.035471	0.44102	-0.07556	0.100358
HNSC	$CD4^+$ T Cell	0.411741	4.59E-21	0.204603	6.22E-06	0.333902	5.78E-14	0.310381	3.53E-12
HNSC	Macrophage	0.168287	0.000203	0.039073	0.391547	0.208927	3.64E-06	0.15759	0.000509
HNSC	Neutrophil	0.254954	1.52E-08	0.094351	0.039001	0.085893	0.060322	0.102868	0.024356
HNSC	Dendritic Cell	0.256053	1.18E-08	0.084101	0.065056	0.206335	4.94E-06	0.141114	0.001899
LIHC	Purity	0.044941	0.404645	0.206513	0.000109	0.035781	0.507094	-0.03814	0.479429
LIHC	B Cell	0.038534	0.476238	0.060448	0.263529	0.24558	4.05E-06	0.207557	0.000105
LIHC	$CD8^+$ T Cell	0.010358	0.848645	-0.00032	0.995289	0.245128	4.50E-06	0.102101	0.059267
LIHC	$CD4^+$ T Cell	0.247894	3.26E-06	0.097734	0.070229	0.391745	4.59E-14	0.466586	5.34E-20
LIHC	Macrophage	0.231972	1.51E-05	0.140673	0.009293	0.43561	3.18E-17	0.285222	8.35E-08
LIHC	Neutrophil	0.300442	1.25E-08	0.215461	5.46E-05	0.532128	1.29E-26	0.311518	3.36E-09
LIHC	Dendritic Cell	0.165791	0.002162	0.04288	0.430624	0.369777	1.86E-12	0.260777	1.09E-06
LUAD	Purity	0.003754	0.933667	-0.09085	0.04356	-0.02825	0.53104	0.024741	0.583283
LUAD	B Cell	0.097083	0.032733	0.015321	0.736719	0.058396	0.199674	0.069707	0.12566
LUAD	$CD8^+$ T Cell	0.099856	0.027561	0.195701	1.36E-05	0.348356	2.43E-15	-0.22863	3.39E-07
LUAD	$CD4^+$ T Cell	0.2445	5.09E-08	0.150368	0.000905	0.230098	3.09E-07	0.312485	2.01E-12
LUAD	Macrophage	0.070577	0.120611	0.199966	9.11E-06	0.328253	1.20E-13	0.069055	0.128844
LUAD	Neutrophil	0.213188	2.27E-06	0.291469	6.51E-11	0.432165	2.13E-23	0.090452	0.046944
LUAD	Dendritic Cell	0.158677	0.000434	0.333937	3.55E-14	0.376147	7.56E-18	0.119594	0.008178
SKCM	Purity	0.174773	0.000171	0.095444	0.041184	0.115416	0.013454	0.114825	0.013941
SKCM	B Cell	0.141423	0.002699	0.006409	0.892392	0.161878	0.000583	-0.05476	0.247378
SKCM	$CD8^+$ T Cell	0.267948	1.23E-08	0.173336	0.000267	0.429439	4.41E-21	-0.17202	0.000298
SKCM	$CD4^+$ T Cell	0.160056	0.000692	-0.03676	0.438668	0.181372	0.000117	0.125096	0.008173
SKCM	Macrophage	0.192654	3.66E-05	0.017963	0.702981	0.339861	1.04E-13	-0.07099	0.131365
SKCM	Neutrophil	0.314276	8.08E-12	0.099757	0.033982	0.557555	2.79E-38	-0.16288	0.000508
SKCM	Dendritic Cell	0.233133	6.41E-07	0.053172	0.262473	0.26107	2.20E-08	0.029562	0.533491

SKCE, Skin cutaneous melanoma; LUAD, Lung adenocarcinoma; LIHC, Liver hepatocellular carcinoma; HNSC, Head and neck cancer; GBM, glioblastoma; BRCA, Breast invasive carcinoma; COAD, colon adenocarcinoma.

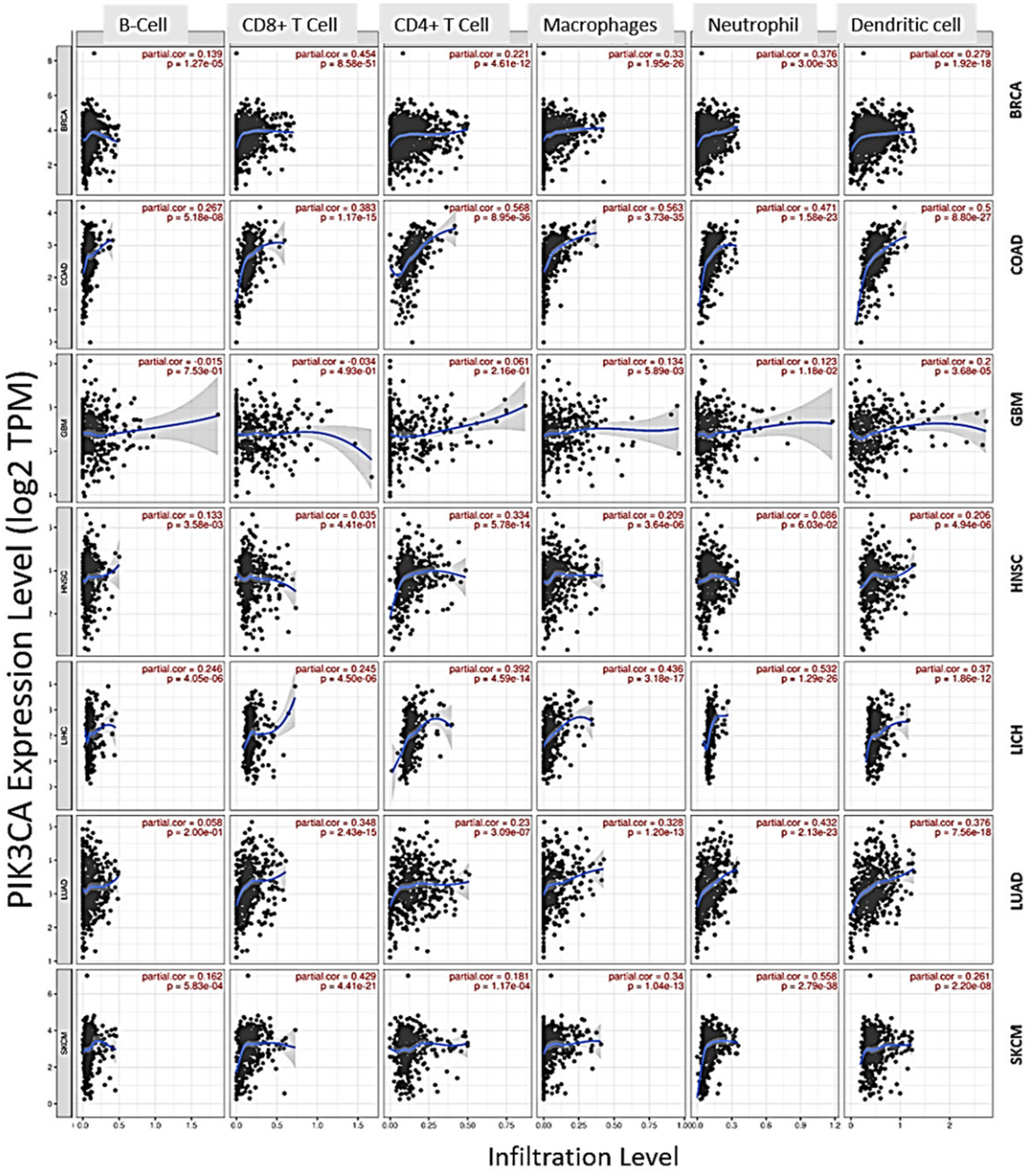

Supplementary Figure 4. Scatterplots of PIK3CA expression correlations with infiltrations of various immune cells in multiple cancer types. The strength of correlations is reflected by the purity-adjusted partial spearman's rho value, where a value of $r = 1$ means a perfect positive correlation and a value of $r = -1$ means a perfect negative correlation. SKCE, Skin cutaneous melanoma; LUAD, Lung adenocarcinoma; LIHC, Liver hepatocellular carcinoma; HNSC, Head and neck cancer; GBM, glioblastoma; BRCA, Breast invasive carcinoma; COAD, colon adenocarcinoma.

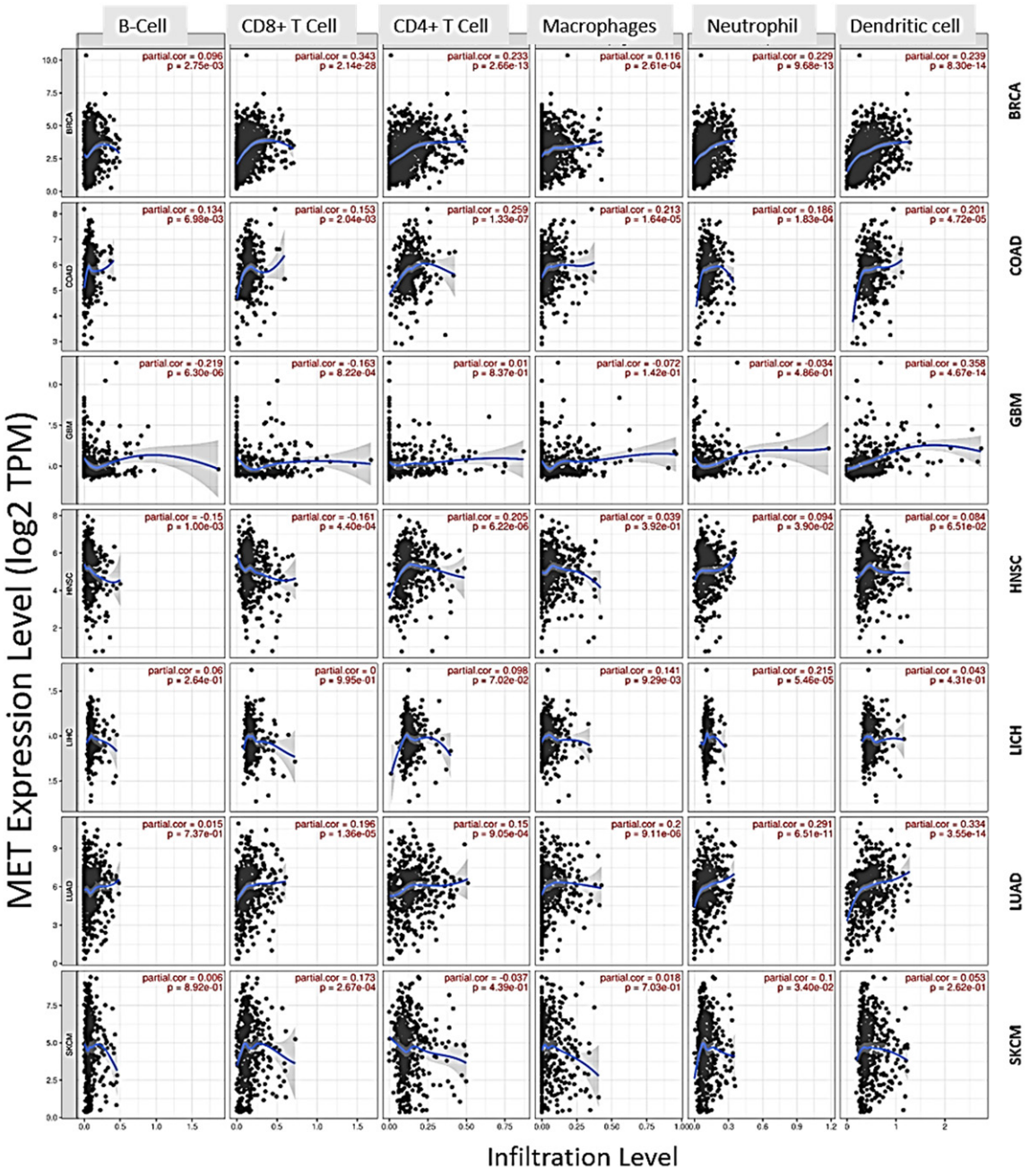

Supplementary Figure 5. Scatterplots of MET expression correlations with infiltrations of various immune cells in multiple cancer types. The strength of correlations is reflected by the purity-adjusted partial spearman's rho value, where a value of $r = 1$ means a perfect positive correlation and a value of $r = -1$ means a perfect negative correlation. SKCE, Skin cutaneous melanoma; LUAD, Lung adenocarcinoma; LIHC, Liver hepatocellular carcinoma; HNSC, Head and neck cancer; GBM, glioblastoma; BRCA, Breast invasive carcinoma; COAD, colon adenocarcinoma.

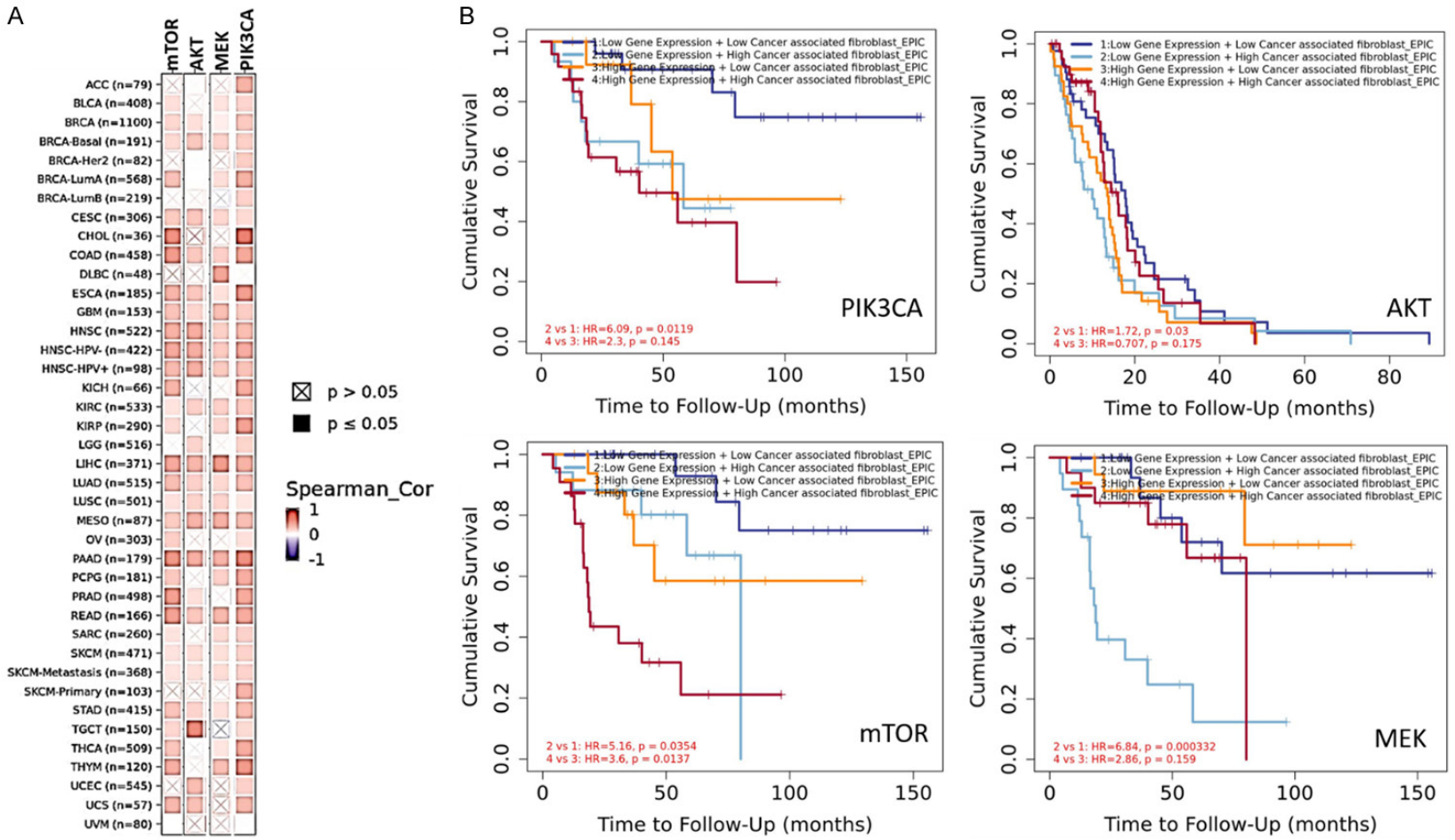

Supplementary Figure 6. PI3K/AKT/mTOR-MEK expressions were associated with cancer-associated fibroblast (CAF) infiltration. (A) Heat map showing correlations of PI3K/AKT/mTOR-MEK expressions and CAF infiltration in multiple cancer types. (B) Kaplan-Meier curve of cumulative survival of cancer cohorts with PI3K/AKT/mTOR-MEK associations. All cohorts were grouped into 4; ^{low}CAF + ^{low}PI3K/AKT/mTOR-MEK, ^{low}CAF + ^{high}PI3K/AKT/mTOR-MEK, ^{high}CAF + ^{low}PI3K/AKT/mTOR-MEK, and ^{high}CAF + ^{high}PI3K/AKT/mTOR-MEK.

Supplementary Table 2. Correlations of PI3K/AKT/mTOR/MET expressions with cancer associated fibroblast infiltrations in multiple cancer types

cancer	MTOR-CAF		AKT-CAF		MEK-CAF		PIK3CA-CAF	
	rho	p	rho	p	rho	p	rho	p
ACC (n = 79)	0.147397	0.213339	0.025849	0.828148	0.13382	0.25902	0.17388	0.125387
BLCA (n = 408)	0.154837	0.0029	0.085708	0.100676	0.136266	0.008861	0.168734	0.000621
BRCA (n = 1100)	0.19407	6.84E-10	0.155633	8.20E-07	0.082452	0.009304	0.211314	1.44E-12
BRCA-Basal (n = 191)	0.176897	0.01954	0.267856	0.000352	0.213694	0.004636	0.227509	0.00155
BRCA-Her2 (n = 82)	0.137196	0.250466	-0.00981	0.93481	0.153793	0.197111	0.120623	0.280378
BRCA-LumA (n = 568)	0.298174	4.47E-12	0.002445	0.955765	0.160399	0.00025	0.313698	1.95E-14
BRCA-LumB (n = 219)	0.09776	0.17734	0.078059	0.281838	-0.08549	0.238411	0.171355	0.011081
CESC (n = 306)	0.254321	1.83E-05	0.274499	3.53E-06	0.194486	0.00114	0.21204	0.000187
CHOL (n = 36)	0.544746	0.000716	0.2866	0.095079	0.142551	0.413987	0.55444	0.00045
COAD (n = 458)	0.490603	4.62E-18	0.263781	9.29E-06	0.228512	0.000132	0.506658	4.69E-20
DLBC (n = 48)	0.237862	0.134252	0.148062	0.355567	0.437808	0.0042	0.258142	0.076482
ESCA (n = 185)	0.3648	4.78E-07	0.272988	0.000209	0.146813	0.049224	0.350031	1.04E-06
GBM (n = 153)	0.291608	0.000545	0.200886	0.018582	0.308705	0.000242	0.190687	0.018224
HNSC (n = 522)	0.376775	4.84E-18	0.404201	9.23E-21	0.234271	1.47E-07	0.368248	3.29E-18
HNSC-HPV- (n = 422)	0.419665	1.70E-18	0.393756	2.76E-16	0.256524	1.97E-07	0.418456	2.55E-19
HNSC-HPV+ (n = 98)	0.333005	0.001429	0.387545	0.000175	0.251085	0.017625	0.326779	0.001023
KICH (n = 66)	0.364962	0.002797	-0.08075	0.522536	0.086822	0.49164	0.339467	0.005296
KIRC (n = 533)	0.131109	0.004809	0.222365	1.42E-06	0.222626	1.38E-06	0.130166	0.002605
KIRP (n = 290)	0.179534	0.003812	-0.06293	0.314021	0.200673	0.001193	0.183295	0.001721
LGG (n = 516)	-0.02749	0.548846	0.20773	4.65E-06	0.066395	0.147221	-0.05387	0.221846
LIHC (n = 371)	0.423837	1.79E-16	0.357385	7.85E-12	0.484599	1.02E-21	0.363563	4.91E-13
LUAD (n = 515)	0.315162	7.87E-13	0.222359	6.13E-07	0.186478	3.09E-05	0.305772	1.31E-12
LUSC (n = 501)	0.142252	0.001842	0.209657	3.87E-06	0.202484	8.31E-06	0.085747	0.055108
MESO (n = 87)	0.250793	0.020608	0.371036	0.000473	0.384602	0.000279	0.278395	0.009028
OV (n = 303)	0.229112	0.000267	0.116878	0.065573	0.11035	0.08224	0.179859	0.001669
PAAD (n = 179)	0.509481	1.11E-12	0.390765	1.26E-07	0.370361	6.16E-07	0.54118	5.23E-15
PCPG (n = 181)	0.265938	0.000513	0.097618	0.209467	0.224424	0.003549	0.267019	0.000279
PRAD (n = 498)	0.472892	1.44E-24	0.153245	0.00172	0.083965	0.087186	0.454204	1.02E-26
READ (n = 166)	0.464692	3.95E-06	0.274591	0.008815	0.351163	0.00069	0.5167	9.75E-08
SARC (n = 260)	0.13508	0.034956	0.110623	0.084634	0.180578	0.004662	0.107071	0.084869
SKCM (n = 471)	0.140552	0.002601	0.163818	0.000438	0.149193	0.001381	0.091886	0.046253
SKCM-Metastasis (n = 368)	0.136383	0.0102	0.150448	0.004557	0.164405	0.001913	0.104806	0.044514
SKCM-Primary (n = 103)	0.184204	0.063835	0.164543	0.098411	0.125997	0.207	0.103359	0.298824
STAD (n = 415)	0.286818	1.31E-08	0.207435	4.71E-05	0.149043	0.003635	0.277667	8.77E-09
TGCT (n = 150)	0.195032	0.017922	0.562151	1.27E-13	-0.15464	0.061459	0.218109	0.007334
THCA (n = 509)	0.275797	5.74E-10	-0.0472	0.29805	0.124423	0.005919	0.278537	1.60E-10
THYM (n = 120)	0.390641	1.59E-05	0.07964	0.397517	0.310806	0.000723	0.377728	2.11E-05
UCEC (n = 545)	0.167367	0.119088	0.323702	0.002095	0.206614	0.053435	0.135943	0.072019
UCS (n = 57)	0.34745	0.0108	0.312884	0.022541	0.224849	0.105513	0.373801	0.00418
UVM (n = 80)	0.002367	0.9837	0.201656	0.078629	0.163206	0.156122	0.022082	0.845848

Supplementary Table 3. Biological Activity Spectra (PASS) of NSC777213

Pa	Pi	Activity
0.631	0.005	Biliary tract disorders treatment
0.43	0.059	Analgesic
0.413	0.052	Autoimmune disorders treatment
0.408	0.064	Neurodegenerative diseases treatment
0.412	0.089	Antiinflammatory
0.371	0.058	Antiinfective
0.309	0.052	Antineoplastic (pancreatic cancer)
0.379	0.128	Antineoplastic (non-Hodgkin's lymphoma)
0.301	0.054	Rheumatoid arthritis treatment
0.314	0.072	Antimycobacterial
0.363	0.139	Antiviral (Rhinovirus)
0.291	0.068	Antiparkinsonian
0.238	0.051	Antineoplastic (colorectal cancer)
0.222	0.05	Antineoplastic (colon cancer)
0.232	0.086	Antipyretic
0.255	0.114	Antiamyloidogenic
0.25	0.11	Antituberculosic
0.22	0.097	Hepatic disorders treatment
0.196	0.096	Antineoplastic (breast cancer)
0.189	0.109	Antineoplastic enhancer
0.311	0.235	Antineurotic
0.124	0.053	Renal failure treatment
0.171	0.104	Antineoplastic (glioblastoma multiforme)

Pa = probability to be active. Pi = probability of in active.

Supplementary Table 4. PharmMapper identified NSC777213 targets

Pharma Model	Num Feature	Fit	Norm Fit	z-score	Name
2p3g_v	3	2.973	0.9909	1.04924	MAP kinase-activated protein kinase 2
1yxx_v	3	2.966	0.9887	1.05995	Proto-oncogene serine/threonine-protein kinase Pim-1
1pmv_v	3	2.92	0.9733	0.736159	Mitogen-activated protein kinase 10
1uki_v	3	2.908	0.9692	0.789831	Mitogen-activated protein kinase 8
1pme_v	3	2.832	0.944	0.565908	Mitogen-activated protein kinase 1
2uzd_v	3	2.625	0.875	0.25408	Cyclin-A2
2a4z_v	3	2.359	0.7863	0.53929	Phosphatidylinositol-4,5-bisphosphate 3-kinase catalytic subunit gamma isoform
1bl6_v	4	3.137	0.7842	1.31171	Mitogen-activated protein kinase 14
2pe0_v	4	2.946	0.7364	0.867702	3-phosphoinositide-dependent protein kinase 1
2j5f_v	4	2.909	0.7273	0.730122	Epidermal growth factor receptor
2h8h_v	4	2.855	0.7138	0.534064	Proto-oncogene tyrosine-protein kinase Src
1m9j_v	4	2.801	0.7001	0.295964	Nitric oxide synthase, endothelial
2ywp_v	4	2.607	0.6519	0.05184	Serine/threonine-protein kinase Chk1
1vjy_v	4	2.436	0.6089	-1.37204	TGF-beta receptor type-1
2rfn_v	5	2.991	0.5981	0.790519	Hepatocyte growth factor receptor
2rl5_v	5	2.988	0.5975	0.617715	Vascular endothelial growth factor receptor 2
1xo2_v	5	2.855	0.5711	0.526278	Cell division protein kinase 6
2w1e_v	5	2.76	0.552	0.407558	Serine/threonine-protein kinase 6
2f57_v	5	2.724	0.5448	0.145173	Serine/threonine-protein kinase PAK 7
1lv2_v	7	3.529	0.5041	1.34132	Hepatocyte nuclear factor 4-gamma

Supplementary Table 5. Swiss dock binding profile of PI3K/AKT/mTOR/MEK

Targets	Full-Fitness (kcal/mol)	Estimated ΔG (kcal/mol)
	NSC777213	
AKT	-1730.24	-6.67
MTOR (PDB:5WBH)	-3481.25	-7.18
PI3K	-4558.36	-7.68

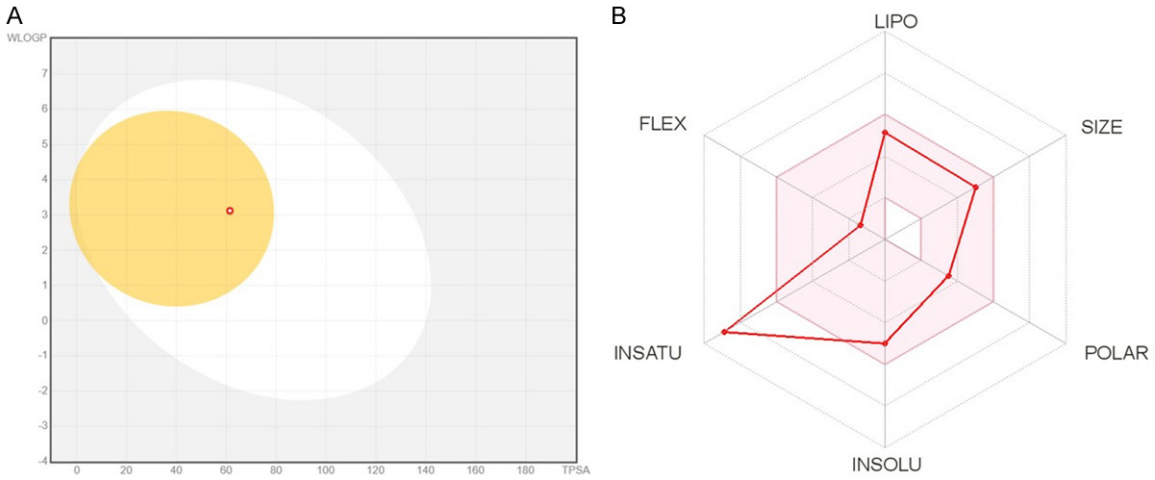

Supplementary Figure 7. (A) Boiled EGG model of BBB permeation and GIA absorption ability of NSC777213 (B) Bioavailability radar of NSC777213.